Atmos. Chem. Phys. Discuss., 15, 35591–35643, 2015
www.atmos-chem-phys-discuss.net/15/35591/2015/
doi:10.5194/acpd-15-35591-2015

Atmospheric Chemistry and Physics Discussions

Model development of dust emission and heterogeneous chemistry within the Community Multiscale Air Quality modeling system and its application over East Asia

X. Dong[1], J. S. Fu[1], K. Huang[1], and D. Tong[2,3,4]

[1]Department of Civil and Environmental Engineering, the University of Tennessee, Knoxville, TN 37996, USA
[2]NOAA/OAR/ARL, NOAA Center for Weather and Climate Prediction, College Park, MD 20740, USA
[3]Center for Spatial Information Science and Systems, George Mason University, Fairfax, VA 22030, USA
[4]Cooperative Institute for Climate and Satellites, University of Maryland, College Park, MD 20740, USA

Received: 22 September 2015 – Accepted: 16 October 2015 – Published: 17 December 2015

Correspondence to: J. S. Fu (jsfu@utk.edu)

Published by Copernicus Publications on behalf of the European Geosciences Union.

ACPD
15, 35591–35643, 2015

Abstract

The Community Multiscale Air Quality (CMAQ) model has been further developed in terms of simulating natural wind-blown dust in this study, with a series of modifications aimed at improving the model's capability to predict the emission, transport, and chemical reactions of dust aerosols. The default parameterization of threshold friction velocity constants in the CMAQ are revised to avoid double counting of the impact of soil moisture based on the re-analysis of field experiment data; source-dependent speciation profiles for dust emission are derived based on local measurements for the Gobi and Taklamakan deserts in East Asia; and dust heterogeneous chemistry is implemented to simulate the reactions involving dust aerosol. The improved dust module in the CMAQ was applied over East Asia for March and April from 2006 to 2010. Evaluation against observations has demonstrated that simulation bias of PM_{10} and aerosol optical depth (AOD) is reduced from −55.42 and −31.97 % in the original CMAQ to −16.05 and −22.1 % in the revised CMAQ, respectively. Comparison with observations at the nearby Gobi stations of Duolun and Yulin indicates that applying a source-dependent profile helps reduce simulation bias for trace metals. Implementing heterogeneous chemistry is also found to result in better agreement with observations for sulfur dioxide (SO_2), sulfate (SO_4^{2-}), nitric acid (HNO_3), nitrous oxides (NO_x), and nitrate (NO_3^-). Investigation of a severe dust storm episode from 19 to 21 March 2010 suggests that the revised CMAQ is capable of capturing the spatial distribution and temporal variations of dust aerosols. Model evaluation indicates potential uncertainties within the excessive soil moisture fraction used by meteorological simulation. The mass contribution of fine mode aerosol in dust emission may be underestimated by 50 %. The revised revised CMAQ provides a useful tool for future studies to investigate the emission, transport, and impact of wind-blown dust over East Asia and elsewhere.

ACPD
15, 35591–35643, 2015

1 Introduction

Natural dust has a wide impact on many different aspects of the Earth's system. It reduces atmospheric visibility (Engelstaedter et al., 2003; Kurosaki and Mikami, 2005; Washington et al., 2003), deteriorates air quality (De Longueville et al., 2010; Prospero, 1999), alters the radiative forcing budget (Liao et al., 2004; Miller et al., 2006; Reddy et al., 2005), and also affects the cloud properties and precipitation (Rosenfeld et al., 2001; Forster et al., 2007). Over East Asia, spring time dust storms often lead to severe air pollution as the intensively elevated aerosol loadings are dumped over the most populated areas. The estimated global source of mineral dust aerosols with diameters below 10 µm is between 1000 and 4000 Tg year^{-1} on a global scale as reported by Intergovernmental Panel on Climate Change (IPCC), and Zhang et al. (2003) reported annual Asian dust emission as about 800 Tg. The dust in East Asia mainly originates from two dominant source regions and their surrounding areas, including the Taklamakan Desert in northwest China and the Gobi Desert in Mongolia and northern China (Huang et al., 2010). In spring, the Mongolian Cyclone associated with the East Asian trough often leads to strong northwesterly near surface winds (Shao and Dong, 2006) that lift and transport the eolia dust particles. East Asian dust can transport to densely populated areas over China (Qian et al., 2002), South Korea (Chun et al., 2001; Park and In, 2003) , and Japan (Ma et al., 2001; Uno et al., 2001), and at times can even transport across the Pacific Ocean, reaching as far as the west coast of North America (Fairlie et al., 2010; Wang et al., 2012; Zhao et al., 2010). Along the transport pathway, mineral dust particles also serve as carriers and reaction platforms by uptaking reactive gases such as ozone (O_3), nitrogen oxides (NO_x), sulfur dioxide (SO_2), nitric acid (HNO_3), hydroxyl radicals (OH), and volatile organic compounds (VOCs). The dust heterogeneous chemistry may change the photochemistry, acid deposition, and production of secondary aerosols. Besides, East Asian dust is believed to contribute geochemically significant amounts of minerals that are deposited into the western part

ACPD
15, 35591–35643, 2015

of the Pacific Ocean. These minerals may alter the oceanic primary productivity (Zhang et al., 2003; Zhuang et al., 1992) as well.

Since natural dust links the biogeochemical cycle of land, atmosphere, and ocean, understanding the emission, evolution, and transport of dust is essential for further examining its impacts on the Earth's system. Numerical modeling is one of the most important approaches for systematically investigating dust. Many global models simulate dust emissions, transport, and depositions. Huneeus et al. (2011) conducted intercomparisons of 15 global models and reported their simulated aerosol optical depth (AOD) and Ångström Exponent (ÅE) within a factor of two and the total deposition and surface concentration within a factor of 10 with respect to observations, indicating significant variations among different models. Regional models usually represent dust by following a coherent manner as global models. For example, the WRF-Chem (Grell et al., 2005) coupled with the GOCART scheme (Ginoux et al., 2001) has been applied to simulate dust emission over Middle-East Asia (Kumar et al., 2014), the United States (Zhao et al., 2010), and East Asia (Chen et al., 2013). The STEM (Carmichael et al., 2003) used the COAMPS scheme (Liu and Westphal, 2001) with application over East Asia (Tang et al., 2004). Regional models have fine spatiotemporal resolution and multiple physical parameterizations at the cost of intensive computation. As compared to global models, regional models may provide more realistic representations of the surface roughness, soil moisture and contents, and also allow comparable validation against surface observations (Darmenova and Sokolik, 2008).

The Community Multiscale Air Quality (CMAQ) model is a state-of-science model and has been applied in numerous regional modeling studies worldwide. Unlike other models in which dust is usually treated as a unique aerosol, the CMAQ distributes dust particles into 19 aerosol species such as inorganic aerosols and trace metals. This method is consistent with the original design of the CMAQ as an air quality model, and it also provides a potential platform to examine the diversities of chemical and physical properties within dust particles. This method also enables the model to examine the mixing status and the net effect of natural dust and anthropogenic aerosols. The vali-

ACPD
15, 35591–35643, 2015

dation of the CMAQ performance is not well understood due to limited research efforts. Appel et al. (2013) conducted a full year simulation with the CMAQ over the continental United States for 2006, and reported good agreement between simulation and observations, with the mean bias around $\pm 0.5\,\mu g\,m^{-3}$ and $0.5–1.5\,\mu g\,m^{-3}$ ($\sim \pm 30\,\%$) for soil concentrations over western and eastern United States, respectively. The CMAQ simulations over other regions underestimate dust emissions significantly. Fu et al. (2014) reported that the default dust scheme in the CMAQ underestimated dust emission by 98 % during a six-day dust storm episode in 2011. With the modeling domain covering the entire Northern Hemisphere, Xing et al. (2015) also suggested that the CMAQ underestimated AOD by 30–60 % in areas where mineral dust is dominant, while the bias was less than ±15 % elsewhere.

The studies mentioned above indicate that the capability of the CMAQ for simulating wind-blown dust remains poorly understood. In addition, the current dust scheme in the CMAQ does not include heterogeneous chemistry treatment of dust particles, while some studies have revealed the important impact of dust chemistry on ambient air pollutants with both measurement (Krueger et al., 2004; Matsuki et al., 2005; Usher et al., 2003) and modeling evidence (Bauer et al., 2004; Bian and Zender, 2003; Dentener et al., 1996). The objective of this study is to evaluate and improve the model's capability of reproducing dust emission, and also enable the model to treat the heterogeneous chemistry of dust particles. Section 2 introduces the method of applying new parameterizations and implementing dust heterogeneous chemistry into the CMAQ, whereas Sect. 3 summarizes the improved model performance based on validation with observations. Section 4 discusses the enhanced model capability and remaining uncertainties, and Sect. 5 concludes the paper with a summary of the findings.

ACPD
15, 35591–35643, 2015

2 Methodology

2.1 Improvement of the CMAQ wind-blown dust emission module

The process of wind-blown dust emission is controlled by a number of environmental variables, including wind speed, soil texture, land use type, vegetation cover, and soil moisture. Dust deflation is favored by dry soil with low and sparse vegetation and constrained by high soil moisture. The dust emission scheme employed in the CMAQ was developed by Tong et al. (2015). The emission (vertical flux) of the dust F ($\mathrm{g\,m^{-2}\,s^{-1}}$) was estimated based on a modified Owen's equation (Owen et al., 1964; Tong et al., 2015):

$$F = \sum_{i=1}^{M}\sum_{j=1}^{N} K \times A \times \frac{\rho}{g} \times S_i \times \mathrm{SEP} \times u_* \times \left(u_*^2 - u_{*ti,j}^2\right) \quad \text{for} \quad u_* > u_{*ti,j} \tag{1}$$

where M is the erodible land use type, N is the soil texture type, K is the ratio of vertical to horizontal flux calculated based on the amount of clay (clay %) within the soil:

$$K = \begin{Bmatrix} 10^{0.134\times(\mathrm{clay}\,\%)-6}, & \text{when: clay}\,\% < 20\,\% \\ 0.0002, & \text{when: clay}\,\% \geq 20\,\% \end{Bmatrix} \tag{2}$$

A is a scaling factor, ρ is air density, g is gravitational acceleration (9.8 $\mathrm{m\,s^{-2}}$), S_i is dust source area for land type i, SEP is the soil erodibility factor, which is calculated based on the amount of clay, silt, and sand of the soil as:

$$\mathrm{SEP} = 0.08 \times \mathrm{clay}\,\% + 1.0 \times \mathrm{silt}\,\% + 0.12 \times \mathrm{sand}\,\% \tag{3}$$

u_* is the friction velocity, and $u_{*ti,j}$ is the threshold friction velocity for soil type j and land use type i. More details of the dust emission algorithm have been given elsewhere (Tong et al., 2015). Equation (1) is applied only when the model calculated friction velocity exceeds the designated threshold value. Therefore, the value of threshold friction

ACPD
15, 35591–35643, 2015

velocity is critical to determine the onset and magnitude of dust emission in the CMAQ model.

In the CMAQ dust module, the threshold friction velocity is dynamically calculated based on the presence of non-erodible elements and the change of soil moisture (Tong et al., 2015). The effect of non-erodible elements is represented by wind energy partitioning following Marticorena et al. (1997). The effect of soil moisture on dust emission is implemented following a two-step approach proposed by Fécan et al. (1999). First, the maximum water holding capacity (W_{max}) for each soil type is determined based on the clay content (clay %) in the soil:

$$W_{max} = (0.0014 \times \text{clay}\,\% + 0.17) \times \text{clay}\,\% \quad (4)$$

In case that soil moisture exceeds W_{max}, the threshold friction velocity is then adjusted using a revised Fecan formulation (Fécan et al., 1999):

$$u_{*ti,j} = u_{*ci,j} \times Z_{i,j} \times f_{S_m i,j} \quad (5)$$

where $u_{*ci,j}$ is the initial threshold friction velocity constant, $Z_{i,j}$ is the surface roughness adjusting factor calculated with surface roughness length from the meteorology field, and $f_{S_m i,j}$ is the moisture adjustment factor calculated as:

$$f_{S_m i,j} = \begin{cases} 999.9, & \text{for } S_m > W_{max} \\ 1.0, & \text{for } S_m \le W_{max} \\ \left(1.0 + 1.21 \times (S_m - W_{max})^{0.68}\right)^{0.5}, & \text{for } S_m \le S_l \end{cases} \quad (6)$$

where S_m is soil moisture, and S_l is the saturation soil moisture limit determined by soil textures.

Previously, the values of initial threshold friction velocity constant were taken from observed data from wind tunnel experiments conducted by Gillette and co-workers

ACPD
15, 35591–35643, 2015

(Gillette et al., 1980, 1982). Fu et al. (2014) found that the initial threshold friction velocity constant $u_{*ci,j}$ used in the CMAQ has an average value of 0.7 m s^{-1} among all soil types, which is too high to generate enough dust particles over East Asia. They used a fixed value of 0.3 m s^{-1} based on a study of local measurements in a northern desert in China (Li et al., 2007). Although this smaller threshold helps to generate higher production of dust emission during the six-day simulation episode from 1 to 6 May 2011, the arbitrarily designated threshold value for all land covers and soil categories prevents the model from reproducing spatial and temporal variations of dust emission. We have conducted a reanalysis of the Gillette field data. While some of these experiments were performed under rather dry conditions, for most of the samples the soil moisture effect cannot be ignored. Therefore, these values reported from field experiments are not always suitable to be used directly as the initial threshold friction velocity constant, which is assumed to represent extremely dry conditions. Meanwhile, in the CMAQ dust module, dynamic soil moisture data are used to adjust threshold friction velocity. Therefore, we need to convert the wet-condition data into threshold values under dry conditions. Otherwise, there will be double counting of soil moistures under some cases. In this study, the revised values of $u_{*ci,j}$ are implemented into the CMAQ. Comparison of the default and revised intital threshold friction velocity constant is summarized in Fig. 1c. As the double-counting of soil moisture has been corrected, the revised constants are lower than the default ones. The majority of land cover in the Gobi is categorized as shrub land, where the revised initial threshold friction velocity constants are significantly lower than the default values for all soil types as shown in Fig. 1c, indicating that the revised scheme is expected to produce more dust emission over the Gobi. The Taklamakan Desert is mainly configured as barren or sparsely vegetated land cover with sandy soil type, which only shows a small drop of the threshold friction velocity constant from 0.28 to 0.23 m s^{-1}. The CMAQ distributes dust emission to four size bins: 0.1–1.0 µm, 1.0–2.5 µm, 2.5–5.0 µm, and 5.0–10.0 µm with the mass distributed as 3, 17, 41, and 39 % for each bin, respectively. The first two bins repre-

ACPD
15, 35591–35643, 2015

sent the fine mode aerosol and the larger two represent the coarse mode. So the mass contribution is 20 % for fine mode and 80 % for the coarse model aerosol.

2.2 Implementing source dependent speciation profile

The emission of natural wind-blown dust particles is distributed to several aerosol species in the CMAQ following the profile developed based on the EPA's SPECIATE database (Simon et al., 2010). As compared with other models that treat dust as a unique aerosol species, the CMAQ approach provides a more detailed description of the chemical components within dust. However, mass contributions of the chemical components may differ greatly among different source areas, thus using a fixed profile within the model for all dust sources may introduce uncertainty and lose the capacity of modeling the varieties of dust. The mass contribution of Aluminum (Al) is 5–8 % for pure minerals around the world, and the ratios between other trace metals and Al could vary substantially for different dust samples. Thus the elemental mass ratio between Calcium and Aluminum (Ca/Al) is usually used to identify the source region of dust sample (Huang et al., 2010; Sun et al., 2005). For example, the Ca/Al ratio for Saharan dust is around 0.9 and 1.0 for fine and coarse dust particles, respectively (Blanco et al., 2003; Formenti et al., 2003; Kandler et al., 2007; Reid et al., 2003); for Arabian dust is around 0.13 and 0.15 for coastal and inland dust, respectively (Krueger et al., 2004); for Taklamakan dust is about 1.5–1.9 (Huang et al., 2010); and for Gobi dust is 0.4–1.1 (Arimoto et al., 2006; Zhang et al., 2003). To characterize the dust aerosols in the CMAQ better, source-dependent speciation profiles are developed in this study for the Gobi and Taklamakan deserts based on local measurement data collected by Huang et al. (2010). These two profiles are compared with the default one in the CMAQ as shown in Table 1. For the model species which are not measured in Huang et al. (2010), including primary organic carbons (APOC), non-carbon aerosols (APNCOM), elementary carbons (EC), silicon (ASI), and water (AH2O), their values for the Taklamakan and Gobi are kept the same as in the default profile. And for unspeciated (AOTHR) and non-anion dust (ASOIL), their values in the two new profiles

ACPD
15, 35591–35643, 2015

are calculated based on the contributions of all other species, to keep the total mass contributions conservative. It is important to notice that the model species refer to an anion or cation phase for sulfate (SO_4^{2-}, ASO4), nitrate (NO_3^-, ANO3), chloride (Cl^-, ACL), ammonium (NH_4^+, ANH4), sodium (Na^+, ANA), Ca_2^+ (ACA), magnesium (Mg_2^+, AMG), and potassium (K^+, AK), and an element phase for iron (Fe, AFE), Al, silicon (Si, ASI), titanium (Ti, ATI), and manganese (Mn, AMN). Mass contributions of different aerosols differ significantly among the default, Taklamakan, and Gobi profiles as suggested by Table 1. For example, Ca_2^+ accounts for 7.94 % of the total fine particle mass in the default profile, which is much higher than the Taklamakan (2.063 %) and the Gobi (1.788 %); for Mg_2^+, the default profile assumes a zero percentage of mass contribution, and the values for the Taklamakan and Gobi are 0.165 and 0.799 %, respectively; and K^+ contribution within the default profile is 3.77 %, while the Taklamakan is 0.153 % and the Gobi is 0.282 %. Si is one of the most abundant metals in the crust, yet the default speciation profile had an inappropriate assumption as zero Si content in coarse mode dust particles. As no measurements were found for Si over the Taklamakan or Gobi, we used the element ratio of Al/Si as 8/28 % to derive the mass contribution of Si in the coarse model dust particles, which is a conventional approach for trace metal analysis (Huang et al., 2010). Different configurations within the speciation profile will lead to significant differences of model predictions of these trace metals, demonstrated in more detail in Sect. 3.

2.3 Implementation of heterogeneous reactions

The default heterogeneous chemistry scheme within the CMAQ considers the conversions from N_2O_5 to HNO_3, and from NO_2 to HONO and HNO_3. These reactions play an important role in the nighttime production of nitrate aerosols (Dong et al., 2014; Pathak et al., 2011; Pun and Seigneur, 2001). Heterogeneous reactions are treated as irreversible in the model (Davis et al., 2008; Sarwar et al., 2008; Vogel et al., 2003). While dust particles serve as a platform for heterogeneous reaction, they also participate in some of the reactions to uptake the gas-phase species and involve species

ACPD
15, 35591–35643, 2015

conversions. The uptake of gases onto the surface of dust particles is defined by a pseudo-first-order reaction rate K (Dentener et al., 1996; Heikes and Thompson, 1983) calculated as:

$$K = \left(\frac{r_p}{D_g} + \frac{4}{v_g \gamma_g} \right)^{-1} A_p \quad (7)$$

where r_p is the radius of the particle, D_g is the diffusion coefficient of gas molecules, v_g is the mean molecular velocity of gas, A_p is the surface area of the particle, and γ_g is the uptake coefficient for gas. Many research efforts have been devoted to quantify the uptake coefficients of gases on dust particles for different reactions. The reported values of the uptake coefficient may differ by more than 2–3 orders of magnitude, depending on the source of the dust samples and analytical methods (Cwiertny et al., 2008; Usher et al., 2003). While this work focuses on East Asia, most of the uptake coefficients are collected from Zhu et al. (2010), which summarized the estimations for dust samples from deserts in China. The "best guess" of uptake coefficients are suggested based on the analysis of different measurement studies summarized in Zhu et al. (2010). But in this study both the lower and upper limits of uptake coefficients are examined. Table 2 lists the 13 dust heterogeneous reactions implemented into the CMAQ in this study and the values of uptake coefficients.

2.4 Model inputs, configuration, and simulation scenarios

The CMAQ model simulation uses version 5.0.1. In this study, the CMAQ is configured with the updated 2005 carbon bond gas-phase mechanism (CB05), aerosol module AE6, in-line photolysis calculation and NO emission from lightning, the ACM2 PBL scheme, and the Euler backward iterative (EBI) solver. The modeling domain covers East Asia and Peninsular Southeast Asia as shown in Fig. 2. The CMAQ simulation was performed with a 36 km horizontal grid spacing and 34 vertical layers with a model

ACPD
15, 35591–35643, 2015

top as 50 hPa, with finer resolution at the near surface layers to represent clearly the planetary boundary layer.

The meteorology field is simulated with the Weather Research and Forecasting model (WRFv3.4, Skamarock et al., 2008). Initial and boundary conditions are generated from the GEOS-Chem global model following the routines described in Lam and Fu (2009). Biogenic emission is from MEGAN2.1 (Guenther et al., 2006; Muller et al., 2008), biomass burning emission is from FLAMBE (Reid et al., 2009), and anthropogenic emission is from Zhao et al. (2013) over China and INTEX-B over other countries within the domain. More details about meteorology and emission datasets are described in Dong and Fu (2015a, b).

To examine the performance of the CMAQ model development with revised parameterization and dust heterogeneous reactions, a total of six scenarios are conducted as listed in Table 3. The simulations Dust_Off and Dust_Default are designed to investigate performance of the CMAQ without dust emission and with the default dust plume rise scheme; Dust_Revised is designed to investigate the performance of applying the new parameterization of initial friction velocity threshold constants; Dust_Profile is designed to examine the improvement by applying source-dependent dust composition profiles; and Dust_Chem and Dust_ChemHigh are designed to examine the impacts of implementing heterogeneous chemistry with lower and upper estimations of uptake coefficients, respectively.

2.5 Observations

Both ground-based measurements and satellite observations are used in this study to help examine the uncertainty and evaluate the performance of the model. The Air Pollution Index (API, http://datacenter.mep.gov.cn) reported by the Chinese Ministry of Environmental Protection (MEP) is used to evaluate the PM_{10} predictions from the CMAQ. The API is reported on a daily basis with a national coverage of 86 middle size or larger cities in China and has been applied in many modeling studies for evaluation purposes (Zhao et al., 2013). To investigate the transport of dust particles over

ACPD
15, 35591–35643, 2015

downwind areas simulated by the model, we also used surface observations from the Acid Deposition Monitoring Network in East Asia (EANET; EANET, 2007) over Japan, and observations from the Taiwan Air Quality Monitoring Network (TAQMN; http://taqm.epa.gov.tw/taqm/en/default.aspx). EANET provides hourly or daily records of PM_{10}, ozone (O_3), nitrous oxides (NO_x), and sulfur dioxide (SO_2), and also bi-weekly (or longer interval) records of HNO_3, sulfate (SO_4^{2-}), and nitrate (NO_3^-), which are also employed in this study for examining model performance with dust chemistry. The TAQMN provides observations of most criteria air pollutants but only PM_{10} observations at the Xinzhuang site are used in this study to focus on the dust impact. Ground-based measurements of K^+, Mg_2^+, Ca_2^+, and $PM_{2.5}$ at Duolun and Yunlin from Fudan University's observation network (Huang et al., 2010) are used to investigate the model's capability of simulating tracer metals by applying the source-dependent speciation profile for suspended dust particles. AOD from the AErosol RObotic NETwork (AERONET; http://aeronet.gsfc.nasa.gov/) operated by NASA is also collected to evaluate the CMAQ predictions. To examine the spatial distribution and column density of model-simulated dust particles, we also used AOD products from the Moderate Resolution Imaging Spectroradiometer (MODIS; http://modis.gsfc.nasa.gov/). The locations of observational stations by the API, EANET, TAQMN, and AERONET are indicated in Fig. 2, along with the locations of Duolun and Yunlin. Table 4 summarizes the detailed information of each observation network.

3 Results

3.1 Improved model performance with revised friction velocity thresholds

To examine model improvement by implementing new initial threshold friction velocity constants, simulation results from Dust_Default and Dust_Revised are compared for the spatial distribution of PM_{10} prediction and evaluation bias against API. Concentration differences of Dust_Default – Dust_Off, and Dust_Revised – Dust_Off represent

ACPD
15, 35591–35643, 2015

the PM_{10} generated by dust from the default dust scheme and the revised dust scheme, respectively, as shown in Fig. 3a and b. PM_{10} concentrations are averaged for March and April from 2006 to 2010. Figure 3a shows that the default dust scheme produces a very limited amount of PM_{10} only over the Gobi Desert for less than 70 $\mu g\,m^{-3}$, which can hardly represent the impacts of spring dust storms over the downwind regions of eastern and southern China. The revised scheme produces high PM_{10} concentrations as more than 400 $\mu g\,m^{-3}$ at the Gobi source region, as indicated in Fig. 3b. Dust plumes are generated by the model over the Gobi and Taklamakan deserts, and also from sparse grassland over the northwest region of the Tibetan Plateau. Particles from dust plumes are transported southeastwardly and contributed 50–100 $\mu g\,m^{-3}$ of PM_{10} over northern and eastern China, and less than 50 $\mu g\,m^{-3}$ over southern China, South Korea, and Japan. Huang et al. (2010) demonstrated that there are two transport pathways for Asian dust: plumes from the Gobi and Taklamakan are either pushed by prevailing winds eastward towards South Korea and Japan or southeastward down towards southern China and Taiwan. The revised CMAQ reproduces the spatial distribution of Asian dust in spring. Figure 3b shows the most significant impact over northern and eastern China and relatively weak impacts over downwind areas as the plume moves eastwards and southwards. Figure 3c and d shows the evaluation bias at the API sites over China for the Dust_Default and Dust_Revised scenarios, respectively. With the default dust scheme, the CMAQ shows a large negative bias for the entire domain. Most serious underestimation is found over northern and western China, with a negative bias more than $-80\,\mu g\,m^{-3}$. Figure 3c also suggests that cities closer to the Taklamakan and Gobi deserts have larger negative bias, indicating that the default scheme cannot generate sufficient dust emission to reproduce the observed PM_{10} levels. With the revised scheme as shown in Fig. 3d, simulation biases for most of the cities are reduced within $\pm 20\,\mu g\,m^{-3}$. The largest overestimation is found at Hohhot as 39 $\mu g\,m^{-3}$, with relatively larger discrepancy in cities close to the Gobi Desert. The largest underestimation was found at Xining and Lanzhou ($-60\,\mu g\,m^{-3}$).

ACPD
15, 35591–35643, 2015

Figure 4a–c summarizes the evaluation statistics for simulated PM_{10} against observations from the API. For the Dust_Off scenario, the CMAQ simulation underestimates PM_{10} concentration by −56.74 %. Since dust storms significantly affect the suspended particle concentrations over East Asia during spring, simulation without dust emission should be responsible for the large underestimation of Dust_Off scenario. With the default dust emission module, model performance for the Dust_Default scenario is only slightly improved and PM_{10} is still underestimated by −55.42 %, as shown by Fig. 4b. The comparison between Dust_Off and Dust_Default suggest that the default dust module is unable to generate sufficient elevated particles to match the observed PM_{10} levels from the API. On the other hand, the Dust_Revised scenario showes a much better performance with a NMB value of −16.06 % as shown in Fig. 4c. To understand better the improvement of the model performance with revised dust scheme for fine particles, simulation results are also evaluated against AOD observations from the AERONET, with the statistics shown in Fig. 4d–f. Statistics for AOD evaluation against the AERONET suggest similar model performances as for PM_{10}. The CMAQ simulation without dust emission underestimates AOD by −31.34 % at AERONET stations, and the default dust module has almost no improvement for AOD prediction. The Dust_Revised scenario underestimates AOD by −22.1 %, indicating that the revised scheme also improves the model's performance for simulating fine mode aerosol.

3.2 Impacts of applying source-dependent profile

Speciation of dust particles determines the contributions of crust species and trace metal concentrations predicted by the model. As described in Sect. 2.2, we modified the fixed speciation profile within the CMAQ based on the source-dependent profiles. In this section the ground-based observations collected at Duolun and Yulin are used to investigate the impacts by applying these profiles. The model simulations from the Dust_Revised and Dust_Profile scenarios are compared with observations for K^+, Mg^+_2, and Ca^+_2 as shown in Fig. 5 (simulations and observations for K^+ and Mg^+_2 are upscaled by 5 and 10 times, respectively, to make them comparable with Ca^+_2 in the same fig-

ACPD
15, 35591–35643, 2015

ure), and evaluation statistics are summarized in Table 5. The two cities are close to the Gobi Desert, as shown by Fig. 1. Huang et al. (2010) used back trajectory and Ca/Al ratio analysis to demonstrate that the Gobi Desert is the main contributor for dust at Duolun and Yulin. Figure 5a indicates that with the default speciation profile, the CMAQ overestimates K^+ and Ca_2^+ by 208.9 and 36.69 %, respectively. Predicted Mg_2^+ concentration is almost zero because there is no anthropogenic emission of Mg_2^+, and the default profile indicates zero mass contribution of Mg_2^+ within dust emission. With the source-dependent speciation profile as shown in Fig. 5b, simulated Mg_2^+ concentration increases significantly and agrees better the observation. Concentrations of K^+ and Ca_2^+ are underestimated by −47.83 and −53.12 %, respectively. Consistent negative bias for trace metals may be due to the underestimation of total fine particles from dust. Figure 5c shows the comparison between observed and simulated $PM_{2.5}$ concentrations at Duolun and Yulin. The Dust_Revised and Dust_Profile scenarios only differ in terms of their speciation profile for particles and the predicted $PM_{2.5}$ from the two scenarios are almost identical, so only one set of data pairs are shown in Fig. 5c. On the one hand, concentration of $PM_{2.5}$ is underestimated by −45.59 % as summarized in Table 5, which is consistent with the underestimation of trace metals. On the other hand, simulation bias shown in Fig. 3d suggests a slight overestimation of PM_{10} at the cities close to the Gobi Desert. So it is highly possible that fine particle mass contribution configured within the CMAQ is underestimated. Unfortunately, no PM_{10} observation is found at Duolun and Yulin. The comparison between the Dust_Revised and Dust_Profile scenarios suggests that the source-dependent speciation profile is more reasonable for predicting trace metals from dust emission.

3.3 Impacts of heterogeneous chemistry

Dust heterogeneous chemistry involves uptake gas-phase species and production of secondary inorganic aerosols. In this section we investigated the impacts of implementing dust chemistry into the CMAQ by evaluating the difference between Dust_Chem and Dust_Profile, and the difference between Dust_ChemHigh and Dust_Profile sce-

ACPD
15, 35591–35643, 2015

narios. Figure 6 demonstrates the concentration changes (color contours represent the absolute concentration changes, and dash lines represent the percentage changes) under the heterogeneous chemistry with lower (left column) and upper (right column) limits of uptake coefficients for O_3 (1st row), SO_2 (2nd row), SO_4^{2-} (3rd row), HNO_3 (4th row), NO_x (5th row), and NO_3^- (6th row). All variables are averaged for March and April from 2006 to 2010. The spatial distributions shown in Fig. 6 suggest that impacts of dust chemistry are more pronounced in eastern China over the downwind areas than that iin the deserts. This is because eastern China has intense anthropogenic emissions that accelerates the dust chemistry, while the deserts have much lower concentrations of the tracer gases. Dong and Fu (2015a) reported that in spring, O_3 concentration is around 30 ppbv and less than 5 ppbv for NO_2 and SO_2 over the Gobi, while the concentrations over eastern China are 50–60 ppbv for O_3 and 10–40 ppbv for NO_2 and SO_2. Li et al. (2012) also reported that the impact of dust chemistry for O_3, SO_2, and NO_2 is less than 5 % over the Gobi but up to 30–40 % in eastern China and even higher over the western Pacific. O_3 concentration is reduced by 3–6 ppbv (2–10 %) and 5–11 ppbv (4–20 %) with the lower and upper limits of uptake coefficients, respectively, due to irreversible Reaction (R1) listed in Table 2, which agrees well with the values reported by Tang et al. (2004) as 20 % and Li et al. (2012) as 5–20 %. Wang et al. (2012) reported lower O_3 reduction due to dust chemistry by 3.8 and 7.3 ppbv with lower and upper uptake coefficients, respectively, because of simulating a different year (2001) with a lower baseline O_3 over East Asia. Concentration of SO_2 is reduced by ~ 2 ppbv (10 %) and ~ 6 ppbv (30 %) with lower and upper limits of uptake coefficients, respectively, due to the consumption in Reaction (R13), which also leads to the increase of SO_4^{2-} concentration by $\sim 3 \mu g\,m^{-3}$ (8 %) and more than $5 \mu g\,m^{-3}$ (15 %) under Dust_Chem and Dust_ChemHigh, respectively. Impacts on SO_2 reported by other studies have a moderate difference with a factor of 2 or more, varying from 55 % by Tang et al. (2004) as the highest, 10–20 % as the medium (Li et al., 2012), and 5–8 % as the lowest (Wang et al., 2012). This should be due to the different simulation episodes employed by different studies.Tang et al. (2004) focused on dust episodes only in 2001 with lower

ACPD
15, 35591–35643, 2015

baseline pollutants from anthropogenic emission; Li et al. (2012) simulated 2010 dust episodes; and Wang et al. (2012) simulated 2001 but focused on the entirety of April, where the monthly averages of particles are apparently smaller than values from dust episodes only. Reaction (R7) indicates consumption and Reaction (R11) indicates production of HNO_3, while the net effect of dust chemistry decreases HNO_3 concentration by 0.2–0.8 ppbv (8–30 %) as shown in Fig. 6e and f. Our result is comparable with the values reported by Li et al. (2012) as 5–40 %, but smaller than that reported by Tang et al. (2004) as 30–70 %. Although the Reaction (R9) indicates uptake of NO_x, simulation results suggest that NO_x concentration is increased by 0.2–1 ppbv over eastern China and the western Pacific due to heterogeneous chemistry. The elevation of NO_x concentration should be attributed to the conversion of gas-phase HNO_3 back to NO_x (Yarwood et al., 2005). As a result of excessive SO_4^{2-} production from dust chemistry, concentration of NO_3^- is decreased under the Dust_Chem scenario due to the thermal-dynamic equilibrium between SO_4^{2-}-NH_4^+-NO_3^-. The equilibrium drives the inorganic aerosols to convert from NH_4NO_3 to $(NH_4)_2SO_4$ over eastern China with intensive anthropogenic SO_2 and NO_x but insufficient NH_3 to neutralize all the acid anions. On the other hand, over the western Pacific and Japan, concentration of NO_3^- is increased slightly due to the productions from Reactions (R8) and (R10). So over eastern and central China, NO_3^- evaporates back to HNO_3, which again pushes the gas-phase equilibrium towards production of NO_x, and thus leads to the increase of NO_x but decrease of HNO_3 and NO_3^-. Meanwhile, with the upper limit of uptake coefficients, the production rate of HNO_3 is found to catch up with the removal rate of NO_3^-, which helps to slow down the decrease of NO_3^- over China and accelerate the increase of NO_3^- over the western Pacific and Japan. Our result is consistent with the findings from other studies. Wang et al. (2012) also reported the increase of NO_x and decrease of HNO_3 and NO_3^- concentrations due to dust chemistry over East Asia. Li et al. (2012) reported that NO_3^- concentration with lower uptake coefficient is about 5 $\mu g\,m^{-3}$ (30 %) lower than the base case simulation (with "best guess" uptake coefficient suggested

ACPD
15, 35591–35643, 2015

in Zhu et al., 2010), and NO_3^- predicted by high uptake coefficient is about 12 μg m^{-3} (100 %) higher than the base case at Shanghai and Xiamen.

The impact of dust chemistry shown in Fig. 6 suggests comparable results as other modeling assessments, but very few previous studies incorporated observation data to validate further the impact indicated by the model. To evaluate the model's capability of representing dust chemistry and also determine the best fit values of uptake coefficients, observations from EANET are used to compare with simulations from Dust_Profile, Dust_Chem, and Dust_ChemHigh scenarios. The evaluation statistics are summarized in Table 6. Simulation results from different scenarios for O_3 all agree well with observations as indicated by the statistics. O_3 is overpredicted by 1.26 % without dust chemistry, and underpredicted by −1.97 and −4.43 % with lower and upper uptake coefficients of dust chemistry, respectively. SO_2 is overpredicted in all scenarios, but the NMB value is reduced from 90.7 % without dust chemistry to 69.8 and 63.7 % with lower and upper uptake coefficients, respectively. Evaluation statistics for HNO_3 and NO_x show a similar response as SO_2, where heterogeneous chemistry helps to reduce the overestimations from 109.03 % without dust chemistry to 85.17 and 81.24 % with lower and upper limits of uptake coefficients, respectively. The positive bias for SO_2 and HNO_3 should be attributed to the overestimated anthropogenic emissions (Dong and Fu, 2015a; Wang et al., 2011). For NO_x evaluation, however, model overestimation is increased from 35.61 % under the Dust_Profile scenario to 37.79 and 38.21 % under the Dust_Chem and Dust_ChemHigh scenarios, respectively. Overestimation of NO_x emission should be responsible for the positive bias of simulation as indicated by previous studies (Dong and Fu, 2015a), but implementing dust chemistry into the model leads to larger overprediction of NO_x. Concentration of SO_4^{2-} is underpredicted by 16.28 % without dust chemistry, and the simulation is overpredicted by 13.74 and 29.43 % under Dust_Chem and Dust_ChemHigh scenarios, respectively. For NO_3^- predictions, dust chemistry helps to reduce the underprediction from 13.07 % under the Dust_Profile scenario to −1.97 % under the Dust_Chem scenario. But the simulation is boosted up too much with upper limit of coefficients and it overpredicts NO_3^- con-

ACPD
15, 35591–35643, 2015

centration by 24.09 % under the Dust_ChemHigh scenario. Note that EANET data are collected from Japanese sites so that Dust_Chem and Dust_ChemHigh show consistent increases of NO_3^-, as explained in Fig. 6. Statistics shown in Table 6 suggest that implementing heterogeneous chemistry improves the CMAQ performance for most of the species except O_3 and NO_x. The lower limit of uptake coefficients favors prediction of SO_4^{2-} and NO_3^-, and the upper limit of uptake coefficients has a better prediction for SO_4^{2-} and HNO_3. Although these statistics show competitive performance between Dust_Chem and Dust_ChemHigh, the lower limit of the uptake coefficients might be more appropriate if we consider the uncertainty within the baseline anthropogenic emissions. With both surface observations and satellite retrievals, Dong and Fu (2015a) demonstrated that the CMAQ overpredicted NO_x and SO_2 over East Asia between 2006 and 2010 by around 30 and 20 %, respectively, due to overestimation in anthropogenic emissions, while Wang et al. (2011) also report overestimation of SO_2 by 14 % over China. Implementing dust chemistry helps to reduce simulated concentrations of SO_2, NO_x, and HNO_3, so it can balance part of the positive bias caused by anthropogenic emissions, but the statistics for SO_4^{2-} and NO_3^- indicate that the counter effect caused by using the upper limit of uptake coefficients might be too excessive and push the balance towards overestimation of aerosols as a side effect. Consequently, without explicitly excluding the bias within anthropogenic emissions, no solid conclusion could be achieved regarding the preference of uptake coefficients.

4 Discussion

4.1 Simulating a severe dust storm event

In this section we probe in to the capability of the CMAQ for reproducing dust stoms. Many studies have reported that spring 2010 had the most severe dust storms in recent decades (Bian et al., 2011; Li et al., 2012) due to nation-wide drought in China. PM_{10} observations were more than 1000 $\mu g\,m^{-3}$ at Beijing (Han et al., 2012), 1600 $\mu g\,m^{-3}$ at

ACPD
15, 35591–35643, 2015

Seoul (Tatarov et al., 2012), and1200 $\mu g\,m^{-3}$ at Taiwan (Tsai et al., 2013). These previous studies mainly focused on the impact of this dust episode on a local scale, and the understanding about the emission and transport of the dust event on a regional scale is not well-developed. Here we examined this severe dust event with model simulations, satellite observations, and also surface measurements from multiple networks. Figure 7 displays the MODIS AOD and simulated AOD from the CMAQ Dust_Chem scenario during a severe dust storm episode from 19 March to 21 in 2010. Simulated AOD is derived by following the approach described in Huang et al. (2013) for 11.00 a.m. local time only to accommodate with the nadir view time by the MODIS. Spatial distributions of satellite agree well with the simulation on a daily scale, indicating that the model can generally reproduce the column density and long-range transport of dust particles. As shown in Fig. 7b, the CMAQ simulation suggests substantial dust emission on 19 March over the Gobi desert, and AOD is increased accordingly. The heavy dust emission on 19 March has been identified with OMI by Li et al. (2011), and Fig. 8a also indicates consistently high AOD values around northern China. As the dust plume moved eastwards, both satellite product and simulation suggest that AOD in the eastern coastal is of China is increased from 0.8 on 19 March to more than 2.0 on 20 March. On 21 March, the majority of the dust plume is pushed eastward and increases the local AOD of the West Pacific and Japan.

To further examine the dust event, forward trajectory is analyzed to characterize the transport pathway of dust with the Hybrid Single-Particle Lagrangian Integrated Trajectory (HYSPLIT) model from NOAA/Air Resources Laboratory (Draxler and Rolph, 2015; Rolph, 2015). Movement of air mass is analyzed for 72 h, starting from 00:00 UTC (8:00 local time) on 19 March 2010 at the Gobi, with the forward trajectories shown in Fig. 8f. Air masses at 500 (red line), 1000 (blue line), and 2000 m (green line) move southeastward until 20 March. The higher plume turns east and moves across Japan and the west Pacific, while the lower plumes continued towards the eastern coastal area of China and finally arrive at Taiwan on 21 March. The HYSPLIT trajectory showes consistent movement of dust as indicated by the MODIS and CMAQ.

ACPD
15, 35591–35643, 2015

To understand the impact of dust storms along the transport pathway, we compare the simulated and observed surface level PM_{10} on a daily scale for all of March 2010 at selected cities, as shown in Fig. 8f. Simulations from the Dust_Chem scenario (black lines in Fig. 8a–e and g–o) and the Dust_Off scenario (blue lines in Fig. 8a–e and g–o) are analyzed to examine the improvement of model performance. Temporal variations of PM_{10} with observations from the API (red circles) are examined at Beijing, Lanzhou, Nanjing, Fuzhou, Lianyungang, and Shanghai as shown in Fig. 8a–e and k, respectively. In northern China, PM_{10} concentration increased rapidly from less than 300 $\mu g\,m^{-3}$ on 18 March to more than 600 $\mu g\,m^{-3}$ at Beijing and 480 $\mu g\,m^{-3}$ at Lianyungang on 19 March. In central and eastern China, concentrations of PM_{10} were more than 600 $\mu g\,m^{-3}$ on 21 March at Nanjing and Shanghai. In southern China, PM_{10} was also elevated to around 600 $\mu g\,m^{-3}$ at Xiamen on 22 March. Temporal variation of PM_{10} at these cities suggested that aerosol concentration was elevated with the onset of the dust storm, which moved from the Gobi to southeastern China from 19 March to 21. PM_{10} concentration was decreased down to 300 $\mu g\,m^{-3}$ after the dust event. Lanzhou reached a peak of PM_{10} concentration as 500 $\mu g\,m^{-3}$ on 14 March, which should be attributed to the impact of the dust from the Taklamakan. Ling et al. (2011) also reported an observed 507 $\mu g\,m^{-3}$ PM_{10} on 14 March at Lanzhou. Observations from EANET and the TAQMN are used to investigate the long-range transport of dust over the West Pacific and Taiwan. Temporal variations of PM_{10} at three EANET sites (green diamonds) including Oki, Ogasawara, and Hedo are shown in Fig. 8h–j, respectively. PM_{10} at these sites all showed consistent increase with the onset of dust on 21 March or 22 March. At Xinzhuang, as shown in Fig. 8g, observations from the TAQMN (purple circles) demonstrated that local PM_{10} was increased from less than 100 $\mu g\,m^{-3}$ on 20 March to more than 700 $\mu g\,m^{-3}$ on 21 March due to the severe impact from the dust storm. Simulated PM_{10} from the Dust_Chem scenario agrees well with observations from different networks all over the domain. Predictions from the Dust_Chem and Dust_Off scenarios are almost the same at all stations during the non-dust period from 1 March to 10 March, yet the Dust_Chem scenario is able to reproduce the rapid el-

ACPD
15, 35591–35643, 2015

evation of PM_{10} during the dust event. However, noticeable discrepancy is also found between the Dust_Chem prediction and observations. In general, the CMAQ overpredicted PM_{10} slightly during dust events at most of the API sites in China, but failed to reproduce the high concentrations at Lanzhou before 15 March and after 20 March. To help understand the model performance of predicting fine particles from dust, daily variations of AOD from the AERONET observations and the CMAQ simulations are examined at four cities, including Beijing, the Semi-Arid Climate Observatory Laboratory (SACOL) station at Lanzhou (Ling et al., 2011), Osaka, and EPA-NCU (Taiwan Environment Protection Agency station at National Central University), as show in Fig. 9l–o, respectively. Temporal variations of AOD were consistent with the changes of PM_{10} at these cities. The highest AOD was found on 14 March at SACOL, which was also consistent with the high PM_{10} concentrations at Lanzhou. Moderate underestimations of AOD were also found at Lanzhou and EPA-NCU during the dust event, indicating that fine mode aerosols might be underestimated over this region by the CMAQ. In general, comparisons between the CMAQ and observations from MODIS and surface networks suggest that the revised model is capable of reproducing the severe dust storm event in terms of spatial distribution, transport, and concentration of dust particles.

4.2 Remaining uncertainties within the modeling system

Despite the improvements of model performance demonstrated in the previous sections, it is necessary to note that there are some important remaining uncertainties within the modeling system. The first type of uncertainty is related to the anthropogenic emissions. Since the bias caused by anthropogenic emissions would affect the model performance, it is difficult to distinguish the uncertainty associate with emission from the uncertainty associated with model scheme. Figure 9 displays the dust emission rate ($Tg\,day^{-1}$) from the Dust_Chem scenario (blue rectangles, with blue dash line indicating the trend), simulation bias of PM_{10} at the API stations (red circles, with red dash line indicating the trend), and simulation bias of PM_{10} at EANET stations (green diamonds, with green dash line indicating the trend), with al variables averaged on a monthly

ACPD
15, 35591–35643, 2015

scale. Prediction from the CMAQ suggests a slightly increasing trend of dust emission from 2006 to 2010, which is consistent with the decadal increase of dust reported by Kurosaki et al. (2011) due to changes of soil erodibility over Mongolia and northeastern China. Simulation biases of PM_{10} agree fairly well with the trend of dust emission at both the API and EANET stations, indicating that overall underprediction of PM_{10} over East Asia has a smaller discrepancy for years with stronger dust events. This is also consistent with previous studies (Wang et al., 2011; Dong and Fu, 2015a) which reported a systematic underestimation of anthropogenic emission of primary particles over China.

The second type of uncertainty lies within the friction velocity threshold u_{*t}, which is overestimated due to the excessive soil moisture fraction simulated by the WRF model. Although in this study the CMAQ simulation improved with the revised initial threshold friction velocity constants u_{*c}, there are still non-negligible biases as shown in Sect. 3. Both the five-year average modeling bias shown in Fig. 3d and temporal variations shown in Fig. 8 suggest possible overestimated dust emission from the Gobi and underestimated dust from the Taklamakan. The averaged u_{*t} calculated by the CMAQ is 0.19 and 0.14 $\mathrm{m\,s^{-1}}$ over the Taklamakan and Gobi, respectively. The soil moisture factor f_{S_m} is 1.21 and 1.13 at the Taklamakan and Gob deserti, respectively. As comapred to the Gobi, the Taklamakan requires higher friction velocity to generate dust because of a more significant soil moisture impact. However, some recent field measurement studies suggested that the u_{*t} in the Taklamakan is lower than that over the Gobi. He et al. (2010) conducted measurements at three sites inside the Taklamakan and reported the value of u_{*t} as 0.25, 0.27 $\mathrm{m\,s^{-1}}$, and 0.21 $\mathrm{m\,s^{-1}}$ at three different sites; Yang et al. (2011) also reported the value of u_{*t} as 0.24 $\mathrm{m\,s^{-1}}$ at Tazhong (~ 39.03° N, 83.65° E). For the Gobi, Li and Zhang (2011) reported the value of u_{*t} as 0.34–0.42 $\mathrm{m\,s^{-1}}$ based on measurements made in April 2006 and 2008. Field measurements defined u_{*t} as equal to the value of friction velocity u_* when dust concentration is increased by 20 % for at least one-half hour (Li and Zhang, 2011), thus the reported values of u_{*t} from the measurement studies are higher than the calculations

ACPD
15, 35591–35643, 2015

from the model. But the comparison between the Taklamakan and Gobi measurements suggested that the model may either underestimate at the Gobi or overestimate at the Taklamakan for u_{*t}. Since f_{S_m} is determined by soil moisture fraction, we compare the soil moisture from FNL (NCEP final analysis data) which is used to drive WRF in this study with GLDAS (Global Land Data Assimilation System; Rodell et al., 2004). Figure 10 shows the five-year averages (for March and April) of soil moisture fraction at top 10 cm depth from (a) FNL and (b) GLDAS. Soil moisture is estimated as 10–15 % by FNL at both deserts, while the values from GLDAS are less than 5 % at the Taklamakan and 5–10 % at the Gobi. Zender et al. (2003) reported that soil moisture from NCEP is too high over active dust emission areas and leads to negative AOD bias of the model on a global scale. With the WRF-NMMB/BSC-Dust model, Haustein et al. (2012) conducted simulations with meteorology driven by FNL and GLDAS respectively over north Africa and reported that the predictions with GLDAS had better agreement with the AERONET's AOD observations due to smaller friction velocity and slightly faster surface wind speed due to lower values of soil moisture. But no such sensitivity studies have been made over East Asia, and unfortunately there is no publicly available observation data for the period of 2006–2010 to examine the potential overestimation of soil moisture by FNL in our modeling domain.So more research efforts are required to explicitly verify the uncertainties caused by using FNL soil moisture data.

The last type of uncertainty lies within the mass contribution of fine aerosol within dust emission. Dust emission is distributed to fine and coarse mode aerosos with mass contributions of 20 and 80 %, respectively. In this study however, the ratio of $PM_{2.5}$ / TSP derived from observations at Duolun and Yulin are 0.42 and 0.39, respectively, indicating that fine mode aerosol should have higher mass contribution within East Asian dust. The data from Huang et al. (2010) indicated that the ratio of $PM_{2.5}$ / TSP at Tazhong was 0.45 in spring 2007, which suggested an even higher fine particle mass contribution at the Taklamakan. Model evaluation results shown in Fig. 5 also demonstrate the systematic underestimations of both trace metals and total $PM_{2.5}$ concentrations at both dust source regions and downwind areas, while the concen-

ACPD
15, 35591–35643, 2015

trations of PM_{10} are slightly overestimated near the source region as demonstrated in Fig. 3. Consequently, it is highly possible that the ratio of fine particles within dust emission should be higher. But since TSP also include all large particles > 10μm, observations of both $PM_{2.5}$ and PM_{10} at active dust regions are urgently needed to help clearly characterize the ratio in the model.

5 Summary

Model development has been implemented into the CMAQ in this study. The initial threshold friction velocity constants are revised by removing the double counting of soil moisture in the default parameters; two source-dependent speciation profiles are derived based on local observations and dust heterogeneous chemistry is implemented as well. The CMAQ with its revised dust scheme was applied over East Asia for March and April from 2006 to 2010. Based on model evaluations with observation from both ground-surface networks and satellite retrievals, the revised dust scheme is demonstrated to improve the performance of CMAQ. Evaluation statistics suggested that the simulation bais of PM_{10} and AOD is reduced from −55 and −31 % by the default model to −16 and −22 % bye the revised model, respectively. Applying source dependent speciation profiles significantly improved the model's capability for simulating trace metals. Impact of dust heterogeneous chemistry is also investigated. Although simulations with dust chemistry generally improve the model performance, no solid conclusion could be made with respect to the preference of uptake coefficients. This is because simulation with lower coefficients has better agreement with observations for O_3, SO_4^{2-}, and NO_3^-, while simulation with upper uptake coefficients has better performance for SO_2 and NO_2.

A severe dust storm episode around 19 –21 March 2010 was investigated to examine the model's performance during extreme dust events. The revised CMAQ modeling system successfully reproduced most of the elevated PM_{10} and AOD observations in both near source (China) and downwind areas (Japan and Taiwan). But some no-

ACPD
15, 35591–35643, 2015

table discrepancies are also found, indicating the existence of potential uncertainties within the revised CMAQ system. Comparison of the FNL and GLDAS soil moisture fractions indicated that the excessive soil moisture within FNL should be responsible for the higher friction velocity threshold and lower dust emissions simulated over the Taklamakan. But more sensitive studies with different reanalysis data inputs for WRF and the local soil moisture measurements in the deserts are needed to reach a solid conclusion. In addition, potential uncertainty is also identified within the mass contributions of fine and coarse mode aerosol of dust. Evaluation results indicated consistent underestimation of trace metals and $PM_{2.5}$ by 30–50 % at Duolun and Yulin close to the Gobi desert, yet the PM_{10} are overestimated slightly at adjacent cities. While measurements from Huang et al. (2010) suggested mass contribution as ∼ 40 % of fine particles in TSP, the value of 20 % used in the current CMAQ might be too low for dust emissions from the Gobi and Taklamakan. In summary, the model development employed in this study has been demonstrated to enhance the capability of the CMAQ for simulating dust over East Asia. The revised model can serve as a useful tool for further investigating the impacts of dust on regional climate over East Asia and elsewhere.

Acknowledgements. We thank NASA GSFC (Grant No. NNX09AG75G) and the National Natural Science Foundation of China (Grant No. 41429501) for their funding support. D. Tong is also particularly grateful for his award of a NASA ROSES grant (NNX13AO45G). We would like to acknowledge Edward J. Hyer for providing biomass burning emission, and we thank Keiichi Sato and Ayako Aoyagi from the Asia Center for Air Pollution Research for providing the EANET data. We would like to acknowledge George Lin of the National Center University for providing the AOD observations from Taiwan, and we would also like to acknowledge China MEP and Taiwan EPA for providing the observation data, and thank NASA for providing the AERONET and MODIS data. We thank the National Institute for Computational Sciences (NICS) for providing the computer sources for the model simulations used in this research.

ACPD
15, 35591–35643, 2015

References

Appel, K. W., Pouliot, G. A., Simon, H., Sarwar, G., Pye, H. O. T., Napelenok, S. L., Akhtar, F., and Roselle, S. J.: Evaluation of dust and trace metal estimates from the Community Multiscale Air Quality (CMAQ) model version 5.0, Geosci. Model Dev., 6, 883–899, doi:10.5194/gmd-6-883-2013, 2013.

Arimoto, R., Kim, Y. J., Kim, Y. P., Quinn, P. K., Bates, T. S., Anderson, T. L., Gong, S., Uno, I., Chin, M., Huebert, B. J., Clarke, A. D., Shinozuka, Y., Weber, R. J., Anderson, J. R., Guazzotti, S. A., Sullivan, R. C., Sodeman, D. A., Prather, K. A., and Sokolik, I. N.: Characterization of Asian Dust during ACE-Asia, Global Planet. Change, 52, 23–56, 2006.

Bauer, S. E., Balkanski, Y., Schulz, M., Hauglustaine, D. A., and Dentener, F.: Global modeling of heterogeneous chemistry on mineral aerosol surfaces: influence on tropospheric ozone chemistry and comparison to observations, J. Geophys. Res.-Atmos., 109, D02304, doi:10.1029/2003JD003868, 2004.

Bian, H., Tie, X. X., Cao, J. J., Ying, Z. M., Han, S. Q., and Xue, Y.: Analysis of a Severe Dust Storm Event over China: application of the WRF-Dust Model, Aerosol Air Qual. Res., 11, 419–428, 2011.

Bian, H. S. and Zender, C. S.: Mineral dust and global tropospheric chemistry: relative roles of photolysis and heterogeneous uptake, J. Geophys. Res.-Atmos., 108, 4672, doi:10.1029/2002JD003143, 2003.

Blanco, A., Dee Tomasi, F., Filippo, E., Manno, D., Perrone, M. R., Serra, A., Tafuro, A. M., and Tepore, A.: Characterization of African dust over southern Italy, Atmos. Chem. Phys., 3, 2147–2159, doi:10.5194/acp-3-2147-2003, 2003.

Carmichael, G. R., Tang, Y., Kurata, G., Uno, I., Streets, D., Woo, J. H., Huang, H., Yienger, J., Lefer, B., Shetter, R., Blake, D., Atlas, E., Fried, A., Apel, E., Eisele, F., Cantrell, C., Avery, M., Barrick, J., Sachse, G., Brune, W., Sandholm, S., Kondo, Y., Singh, H., Talbot, R., Bandy, A., Thorton, D., Clarke, A., and Heikes, B.: Regional-scale chemical transport modeling in support of the analysis of observations obtained during the TRACE-P experiment, J. Geophys. Res.-Atmos., 108, 8823, doi:10.1029/2002JD003117, 2003.

Chen, S. Y., Huang, J. P., Zhao, C., Qian, Y., Leung, L. R., and Yang, B.: Modeling the transport and radiative forcing of Taklimakan dust over the Tibetan Plateau: a case study in the summer of 2006, J. Geophys. Res.-Atmos., 118, 797–812, 2013.

ACPD
15, 35591–35643, 2015

Chun, Y. S., Boo, K. O., Kim, J., Park, S. U., and Lee, M.: Synopsis, transport, and physical characteristics of Asian dust in Korea, J. Geophys. Res.-Atmos., 106, 18461–18469, 2001.
Cwiertny, D. M., Young, M. A., and Grassian, V. H.: Chemistry and photochemistry of mineral dust aerosol, Annu. Rev. Phys. Chem., 59, 27–51, 2008.
Darmenova, K. and Sokolik, I. N.: Dust Emission and Deposition in Regional Models, 3rd International Dust Workshop, Leipzig, Germany, 15 September 2008, 01–03, 2008.
Davis, J. M., Bhave, P. V., and Foley, K. M.: Parameterization of N_2O_5 reaction probabilities on the surface of particles containing ammonium, sulfate, and nitrate, Atmos. Chem. Phys., 8, 5295–5311, doi:10.5194/acp-8-5295-2008, 2008.
De Longueville, F., Hountondji, Y. C., Henry, S., and Ozer, P.: What do we know about effects of desert dust on air quality and human health in West Africa compared to other regions?, Sci. Total Environ., 409, 1–8, 2010.
Dentener, F. J., Carmichael, G. R., Zhang, Y., Lelieveld, J., and Crutzen, P. J.: Role of mineral aerosol as a reactive surface in the global troposphere, J. Geophys. Res.-Atmos., 101, 22869–22889, 1996.
Dong, X. Y. and Fu, J. S.: Understanding interannual variations of biomass burning from Peninsular Southeast Asia, part I: Model evaluation and analysis of systematic bias, Atmos. Environ., 116, 293–307, 2015a.
Dong, X. Y. and Fu, J. S.: Understanding interannual variations of biomass burning from Peninsular Southeast Asia, part II: Variability and different influences in lower and higher atmosphere levels, Atmos. Environ., 115, 9–18, 2015b.
Dong, X. Y., Li, J., Fu, J. S., Gao, Y., Huang, K., and Zhuang, G. S.: Inorganic aerosols responses to emission changes in Yangtze River Delta, China, Sci. Total Environ., 481, 522–532, 2014.
Draxler, R. R. and Rolph, G. D.: HYSPLIT (HYbrid Single-Particle Lagrangian Integrated Trajectory) Model access via NOAA ARL READY Website, NOAA Air Resources Laboratory, Silver Spring, MD, USA, available at: http://ready.arl.noaa.gov/HYSPLIT.php, last access: 1 August 2015.
EANET: EANET Data Report 2006, Acid Deposition Monitoring Network in East Aisa (EANET), 2007.
Engelstaedter, S., Kohfeld, K. E., Tegen, I., and Harrison, S. P.: Controls of dust emissions by vegetation and topographic depressions: an evaluation using dust storm frequency data, Geophys. Res. Lett., 30, 1294, doi:10.1029/2002GL016471, 2003.

ACPD
15, 35591–35643, 2015

Fairlie, T. D., Jacob, D. J., Dibb, J. E., Alexander, B., Avery, M. A., van Donkelaar, A., and Zhang, L.: Impact of mineral dust on nitrate, sulfate, and ozone in transpacific Asian pollution plumes, Atmos. Chem. Phys., 10, 3999–4012, doi:10.5194/acp-10-3999-2010, 2010.

Fécan, F., Marticorena, B., and Bergametti, G.: Parametrization of the increase of the aeolian erosion threshold wind friction velocity due to soil moisture for arid and semi-arid areas, Ann. Geophys., 17, 149–157, doi:10.1007/s00585-999-0149-7, 1999.

Formenti, P., Elbert, W., Maenhaut, W., Haywood, J., and Andreae, M. O.: Chemical composition of mineral dust aerosol during the Saharan Dust Experiment (SHADE) airborne campaign in the Cape Verde region, September 2000, J. Geophys. Res.-Atmos., 108, 8576, doi:10.1029/2002JD002648, 2003.

Forster, P., Ramaswamy, V., Artaxo, P., Berntsen, T., Betts, R., Fahey, D. W., Haywood, J., Lean, J., Lowe, D. C., Myhre, G., Nganga, J., Prinn, R., Raga, G., Schulz, M., and Van Dorland, R.: Radiative forcing of climate change, in: Climate Change 2007: The Physical Science Basis. Contribution of Working Group I to the Fourth Assessment Report of the Intergovernmental Panel on Climate Change, edited by: Solomon, S., Qin, D., Manning, M., Chen, Z., Marquis, M., Averyt, K. B., Tignor, M., and Miller, H. L., Cambridge Univ. Press, Cambridge, UK and New York, NY, USA, 129–234, 2007.

Fu, X., Wang, S. X., Cheng, Z., Xing, J., Zhao, B., Wang, J. D., and Hao, J. M.: Source, transport and impacts of a heavy dust event in the Yangtze River Delta, China, in 2011, Atmos. Chem. Phys., 14, 1239–1254, doi:10.5194/acp-14-1239-2014, 2014.

Gillette, D. A., Adams, J., Endo, A., Smith, D., and Kihl, R.: Threshold velocities for input of soil particles into the air by desert soils, J. Geophys. Res.-Oceans, 85, 5621–5630, 1980.

Gillette, D. A., Adams, J., Muhs, D., and Kihl, R.: Threshold friction velocities and rupture moduli for crusted desert soils for the input of soil particles into the air, J. Geophys. Res., 87, 9003–9015, 1982.

Ginoux, P., Chin, M., Tegen, I., Prospero, J. M., Holben, B., Dubovik, O., and Lin, S. J.: Sources and distributions of dust aerosols simulated with the GOCART model, J. Geophys. Res.-Atmos., 106, 20255–20273, 2001.

Grell, G. A., Peckham, S. E., Schmitz, R., McKeen, S. A., Frost, G., Skamarock, W. C., and Eder, B.: Fully coupled "online" chemistry within the WRF model, Atmos. Environ., 39, 6957–6975, 2005.

Guenther, A., Karl, T., Harley, P., Wiedinmyer, C., Palmer, P. I., and Geron, C.: Estimates of global terrestrial isoprene emissions using MEGAN (Model of Emissions of Gases and

ACPD
15, 35591–35643, 2015

Aerosols from Nature), Atmos. Chem. Phys., 6, 3181–3210, doi:10.5194/acp-6-3181-2006, 2006.
Han, X., Ge, C., Tao, J. H., Zhang, M. G., and Zhang, R. J.: Air quality modeling for a strong dust event in East Asia in March 2010, Aerosol Air Qual. Res., 12, 615–628, 2012.
Haustein, K., Pérez, C., Baldasano, J. M., Jorba, O., Basart, S., Miller, R. L., Janjic, Z., Black, T., Nickovic, S., Todd, M. C., Washington, R., Müller, D., Tesche, M., Weinzierl, B., Esselborn, M., and Schladitz, A.: Atmospheric dust modeling from meso to global scales with the online NMMB/BSC-Dust model – Part 2: Experimental campaigns in Northern Africa, Atmos. Chem. Phys., 12, 2933–2958, doi:10.5194/acp-12-2933-2012, 2012.
Heikes, B. G. and Thompson, A. M.: Effects of heterogeneous processes on NO_3, HONO, and HNO_3 chemistry in the troposphere, J. Geophys. Res.-Oceans, 88, 883–895, 1983.
Huang, K., Zhuang, G. S., Li, J. A., Wang, Q. Z., Sun, Y. L., Lin, Y. F., and Fu, J. S.: Mixing of Asian dust with pollution aerosol and the transformation of aerosol components during the dust storm over China in spring 2007, J. Geophys. Res.-Atmos., 115, D00K13, doi:10.1029/2009JD013145, 2010.
Huang, K., Fu, J. S., Hsu, N. C., Gao, Y., Dong, X., Tsay, S.-C., and Lam, Y. F.: Impact assessment of biomass burning on air quality in Southeast and East Asia during BASE-ASIA, Atmos. Environ., 78, 291–302, doi:10.1016/j.atmosenv.2012.03.048, 2013.
Huneeus, N., Schulz, M., Balkanski, Y., Griesfeller, J., Prospero, J., Kinne, S., Bauer, S., Boucher, O., Chin, M., Dentener, F., Diehl, T., Easter, R., Fillmore, D., Ghan, S., Ginoux, P., Grini, A., Horowitz, L., Koch, D., Krol, M. C., Landing, W., Liu, X., Mahowald, N., Miller, R., Morcrette, J.-J., Myhre, G., Penner, J., Perlwitz, J., Stier, P., Takemura, T., and Zender, C. S.: Global dust model intercomparison in AeroCom phase I, Atmos. Chem. Phys., 11, 7781–7816, doi:10.5194/acp-11-7781-2011, 2011.
Kandler, K., Benker, N., Bundke, U., Cuevas, E., Ebert, M., Knippertz, P., Rodriguez, S., Schutz, L., and Weinbruch, S.: Chemical composition and complex refractive index of Saharan Mineral Dust at Izana, Tenerife (Spain) derived by electron microscopy, Atmos. Environ., 41, 8058–8074, 2007.
Krueger, B. J., Grassian, V. H., Cowin, J. P., and Laskin, A.: Heterogeneous chemistry of individual mineral dust particles from different dust source regions: the importance of particle mineralogy, Atmos. Environ., 38, 6253–6261, 2004.
Kumar, R., Barth, M. C., Pfister, G. G., Naja, M., and Brasseur, G. P.: WRF-Chem simulations of a typical pre-monsoon dust storm in northern India: influences on aerosol optical properties

ACPD
15, 35591–35643, 2015

and radiation budget, Atmos. Chem. Phys., 14, 2431–2446, doi:10.5194/acp-14-2431-2014, 2014.
Kurosaki, Y. and Mikami, M.: Regional difference in the characteristic of dust event in East Asia: relationship among dust outbreak, surface wind, and land surface condition, J. Meteorol. Soc. Jpn., 83A, 1–18, 2005.
Lam, Y. F. and Fu, J. S.: A novel downscaling technique for the linkage of global and regional air quality modeling, Atmos. Chem. Phys., 9, 9169–9185, doi:10.5194/acp-9-9169-2009, 2009.
Li, J., Wang, Z., Zhuang, G., Luo, G., Sun, Y., and Wang, Q.: Mixing of Asian mineral dust with anthropogenic pollutants over East Asia: a model case study of a super-duststorm in March 2010, Atmos. Chem. Phys., 12, 7591–7607, doi:10.5194/acp-12-7591-2012, 2012.
Li, J. W., Han, Z. W., and Zhang, R. J.: Model study of atmospheric particulates during dust storm period in March 2010 over East Asia, Atmos. Environ., 45, 3954–3964, doi:10.1016/j.atmosenv.2011.04.068, 2011.
Li, W. Y., Shen, Z. B, Lu, S. H., and Li, Y. H: Sensitivity tests of factors influencing wind erosion, J. Desert Res., 27, 984–993, 2007.
Li, X. and Zhang, H. S.: Research on threshold friction velocities during dust events over the Gobi Desert in northwest China, J. Geophys. Res., 116, D20210, doi:10.1029/2010JD015572, 2011.
Liao, H., Seinfeld, J. H., Adams, P. J., and Mickley, L. J.: Global radiative forcing of coupled tropospheric ozone and aerosols in a unified general circulation model, J. Geophys. Res.-Atmos., 109, D16207, doi:10.1029/2003JD004456, 2004.
Ling, X., Guo, W., Zhao, Q., and Zhang, B.: A case study of a typical dust storm event over the Loess Plateau of northwest China Atmos. Ocean. Sci. Lett., 4, 344–348, 2011.
Liu, M. and Westphal, D. L.: A study of the sensitivity of simulated mineral dust production to model resolution, J. Geophys. Res.-Atmos., 106, 18099–18112, 2001.
Ma, C. J., Kasahara, M., Holler, R., and Kamiya, T.: Characteristics of single particles sampled in Japan during the Asian dust-storm period, Atmos. Environ., 35, 2707–2714, 2001.
Marticorena, B., Bergametti, G., Aumont, B., Callot, Y., N'Doume, C., and Legrand, M.: Modeling the atmospheric dust cycle. 2. Simulation of Saharan dust sources, J. Geophys. Res.-Atmos., 102, 4387–4404, 1997.
Matsuki, A., Iwasaka, Y., Shi, G. Y., Zhang, D. Z., Trochkine, D., Yamada, M., Kim, Y. S., Chen, B., Nagatani, T., Miyazawa, T., Nagatani, M., and Nakata, H.: Morphological and

ACPD
15, 35591–35643, 2015

chemical modification of mineral dust: observational insight into the heterogeneous uptake of acidic gases, Geophys. Res. Lett., 32, L22806, doi:10.1029/2005GL024176, 2005.
Miller, R. L., Cakmur, R. V., Perlwitz, J., Geogdzhayev, I. V., Ginoux, P., Koch, D., Kohfeld, K. E., Prigent, C., Ruedy, R., Schmidt, G. A., and Tegen, I.: Mineral dust aerosols in the NASA goddard institute for Space Sciences ModelE atmospheric general circulation model, J. Geophys. Res.-Atmos., 111, D06208, doi:10.1029/2005JD005796, 2006.
Müller, J.-F., Stavrakou, T., Wallens, S., De Smedt, I., Van Roozendael, M., Potosnak, M. J., Rinne, J., Munger, B., Goldstein, A., and Guenther, A. B.: Global isoprene emissions estimated using MEGAN, ECMWF analyses and a detailed canopy environment model, Atmos. Chem. Phys., 8, 1329–1341, doi:10.5194/acp-8-1329-2008, 2008.
Owen, P. R.: Saltation of uniform grains in air, J. Fluid Mech., 20, 225–242, 1964.
Park, S. U. and In, H. J.: Parameterization of dust emission for the simulation of the yellow sand (Asian dust) event observed in March 2002 in Korea, J. Geophys. Res.-Atmos., 108, 4618, doi:10.1029/2003JD003484, 2003.
Pathak, R. K., Wang, T., and Wu, W. S.: Nighttime enhancement of $PM_{2.5}$ nitrate in ammonia-poor atmospheric conditions in Beijing and Shanghai: plausible contributions of heterogeneous hydrolysis of N2O5 and HNO3 partitioning, Atmos. Environ., 45, 1183–1191, 2011.
Prospero, J. M.: Long-term measurements of the transport of African mineral dust to the southeastern United States: implications for regional air quality, J. Geophys. Res.-Atmos., 104, 15917–15927, 1999.
Pun, B. K. and Seigneur, C.: Sensitivity of particulate matter nitrate formation to precursor emissions in the California San Joaquin Valley, Environ. Sci. Technol., 35, 2979–2987, 2001.
Qian, W. H., Quan, L. S., and Shi, S. Y.: Variations of the dust storm in China and its climatic control, J. Climate, 15, 1216–1229, 2002.
Reddy, M. S., Boucher, O., Balkanski, Y., and Schulz, M.: Aerosol optical depths and direct radiative perturbations by species and source type, Geophys. Res. Lett., 32, L12803, doi:10.1029/2004GL021743, 2005.
Reid, E. A., Reid, J. S., Meier, M. M., Dunlap, M. R., Cliff, S. S., Broumas, A., Perry, K., and Maring, H.: Characterization of African dust transported to Puerto Rico by individual particle and size segregated bulk analysis, J. Geophys. Res.-Atmos., 108, 8591, doi:10.1029/2002JD002935, 2003.
Reid, J. S., Hyer, E. J., Prins, E. M., Westphal, D. L., Zhang, J. L., Wang, J., Christopher, S. A., Curtis, C. A., Schmidt, C. C., Eleuterio, D. P., Richardson, K. A., and Hoffman, J. P.: Global

ACPD
15, 35591–35643, 2015

monitoring and forecasting of biomass-burning smoke: description of and lessons from the Fire Locating and Modeling of Burning Emissions (FLAMBE) Program, IEEE J. Sel. Top. Appl., 2, 144–162, 2009.
Rodell, M., Houser, P. R., Jambor, U., Gottschalck, J., Mitchell, K., Meng, C. J., Arsenault, K., Cosgrove, B., Radakovich, J., Bosilovich, M., Entin, J. K., Walker, J. P., Lohmann, D., and Toll, D.: The global land data assimilation system, B. Am. Meteorol. Soc., 85, 381–394, doi:10.1175/Bams-85-3-381, 2004.
Rolph, G. D.: Real-time Environmental Applications and Display sYstem (READY), NOAA Air Resources, Laboratory, Silver Spring, MD, USA, available at: http://ready.arl.noaa.gov, last access: 1 August 2015.
Rosenfeld, D., Rudich, Y., and Lahav, R.: Desert dust suppressing precipitation: a possible desertification feedback loop, P. Natl. Acad. Sci. USA, 98, 5975–5980, 2001.
Sarwar, G., Roselle, S. J., Mathur, R., Appel, W., Dennis, R. L., and Vogel, B.: A comparison of CMAQ HONO predictions with observations from the northeast oxidant and particle study, Atmos. Environ., 42, 5760–5770, 2008.
Shao, Y. and Dong, C. H.: A review on East Asian dust storm climate, modelling and monitoring, Global Planet. Change, 52, 1–22, 2006.
Simon, H., Beck, L., Bhave, P. V., Divita, F., Hsu, Y., Luecken, D., Mobley, J. D., Pouliot, G. A., Reff, A., Sarwar, G., and Strum, M.: The development and uses of EPA's SPECIATE database, Atmos. Pollut. Res., 1, 196–206, 2010.
Skamarock, W. C., Klemp, J. B., Dudhia, J., Gill, D. O., Barker, D. M., Duda, M. G., Huang, X. Y., Wang, W., and Powers, J. G.: A Description of the Advanced Research WRF Version 3. NCAR, NCAR Technical Note NCAR/TN-475+STR, doi:10.5065/D68S4MVH, 2008.
Sun, Y. L., Zhuang, G. S., Wang, Y., Zhao, X. J., Li, J., Wang, Z. F., and An, Z. S.: Chemical composition of dust storms in Beijing and implications for the mixing of mineral aerosol with pollution aerosol on the pathway, J. Geophys. Res.-Atmos., 110, D24209, doi:10.1029/2005JD006054, 2005.
Tang, Y. H., Carmichael, G. R., Kurata, G., Uno, I., Weber, R. J., Song, C. H., Guttikunda, S. K., Woo, J. H., Streets, D. G., Wei, C., Clarke, A. D., Huebert, B., and Anderson, T. L.: Impacts of dust on regional tropospheric chemistry during the ACE-Asia experiment: a model study with observations, J. Geophys. Res.-Atmos., 109, D19S21, doi:10.1029/2003JD003806, 2004.
Tatarov, B., Muller, D., Noh, Y. M., Lee, K. H., Shin, D. H., Shin, S. K., Sugimoto, N., Seifert, P., and Kim, Y. J.: Record heavy mineral dust outbreaks over Korea in 2010: Two cases observed

ACPD
15, 35591–35643, 2015

with multiwavelength aerosol/depolarization/Raman-quartz lidar, Geophys. Res. Lett., 39, L14801, doi:10.1029/2012GL051972, 2012.
Tsai, F. J., Fang, Y. S., and Huang, S. J.: Case Study of Asian Dust Event on 19–25 March, 2010 and Its Impact on the Marginal Sea of China, J. Mar. Sci. Technol.-Taiwan, 21, 353–360, 2013.
Tong, D. Q., Bowker, G. E., He, S., Byun, D. W., Mathur, R., and Gillette, D. A.: Development of a windblown dust emission model FENGSHAA description and initial application in the United States, in review, 2015.
Uno, I., Amano, H., Emori, S., Kinoshita, K., Matsui, I., and Sugimoto, N.: Trans-Pacific yellow sand transport observed in April 1998: A numerical simulation, J. Geophys. Res.-Atmos., 106, 18331–18344, 2001.
Usher, C. R., Michel, A. E., and Grassian, V. H.: Reactions on mineral dust, Chem. Rev., 103, 4883–4939, 2003.
Vogel, B., Vogel, H., Kleffmann, J., and Kurtenbach, R.: Measured and simulated vertical profiles of nitrous acid – Part II. Model simulations and indications for a photolytic source, Atmos. Environ., 37, 2957–2966, 2003.
Wang, K., Zhang, Y., Nenes, A., and Fountoukis, C.: Implementation of dust emission and chemistry into the Community Multiscale Air Quality modeling system and initial application to an Asian dust storm episode, Atmos. Chem. Phys., 12, 10209–10237, doi:10.5194/acp-12-10209-2012, 2012.
Wang, S. X., Xing, J., Chatani, S., Hao, J. M., Klimont, Z., Cofala, J., and Amann, M.: Verification of anthropogenic emissions of China by satellite and ground observations, Atmos. Environ., 45, 6347–6358, 2011.
Washington, R., Todd, M., Middleton, N. J., and Goudie, A. S.: Dust-storm source areas determined by the total ozone monitoring spectrometer and surface observations, Ann. Assoc. Am. Geogr., 93, 297–313, 2003.
Xing, J., Mathur, R., Pleim, J., Hogrefe, C., Gan, C.-M., Wong, D. C., Wei, C., Gilliam, R., and Pouliot, G.: Observations and modeling of air quality trends over 1990–2010 across the Northern Hemisphere: China, the United States and Europe, Atmos. Chem. Phys., 15, 2723–2747, doi:10.5194/acp-15-2723-2015, 2015.
Yarwood, J., Rao, S., Yocke, Ma., Whitten, G. Z., and Reyes, S.: Updates to the Carbon Bond Mechanism: CB05, Final Report to the US EPA, RT-0400675, Chapel Hill, NC, December, 2005.

ACPD
15, 35591–35643, 2015

Zhang, X. Y., Gong, S. L., Zhao, T. L., Arimoto, R., Wang, Y. Q., and Zhou, Z. J.: Sources of Asian dust and role of climate change versus desertification in Asian dust emission, Geophys. Res. Lett., 30, 2272, doi:10.1029/2003GL018206, 2003.

Zhao, B., Wang, S. X., Dong, X. Y., Wang, J. D., Duan, L., Fu, X., Hao, J. M., and Fu, J.: Environmental effects of the recent emission changes in China: implications for particulate matter pollution and soil acidification, Environ. Res. Lett., 8, 024031, doi:10.1088/1748-9326/8/2/024031, 2013.

Zhao, C., Liu, X., Leung, L. R., Johnson, B., McFarlane, S. A., Gustafson Jr., W. I., Fast, J. D., and Easter, R.: The spatial distribution of mineral dust and its shortwave radiative forcing over North Africa: modeling sensitivities to dust emissions and aerosol size treatments, Atmos. Chem. Phys., 10, 8821–8838, doi:10.5194/acp-10-8821-2010, 2010.

Zhu, H. and Zhang, H. S.: An estimation of the threshold friction velocities over the three different dust storm source areas in northwest China, Acta Meteorol. Sin., 68, 977–984, 2010 (in Chinese).

Zhuang, G. S., Yi, Z., Duce, R. A., and Brown, P. R.: Link between iron and sulfur cycles suggested by detection of Fe(II) in remote marine aerosols, Nature, 355, 537–539, 1992.

ACPD
15, 35591–35643, 2015

Table 1. Dust emission speciation profiles from the default CMAQ, and the profiles derived in this study for the Taklamakan and Gobi deserts. Simulation results of ACA, AMG, and AK (in bold) will be evaluated against observations in next section.

Model Species	Description	Mass contributions (%)					
		Fine Mode (I,J mode in CMAQ ≤ 2.5μm)			Coarse Mode (K mode in CMAQ ≤ 10 μm)		
		Default	Taklamakan	Gobi	Default	Taklamakan	Gobi
ASO4	Sulfate (SO_4^{2-})	2.5	3.554	0.953	2.655	2.825	0.471
ANO3	Nitrate (NO_3^-)	0.02	0.181	0.204	0.16	0.125	0.084
ACL	Chloride (Cl^-)	0.945	2.419	0.544	1.19	2.357	0.094
ANH4	Ammonium (NH_4^+)	0.005	0.098	0.346	0	0.066	0.185
ANA	Sodium (Na^+)	3.935	2.234	1.016	0	2.056	0.301
ACA	**Calcium (Ca_2^+)**	**7.94**	**2.063**	**1.788**	**0**	**1.423**	**1.082**
AMG	**Magnesium (Mg_2^+)**	**0**	**0.165**	**0.799**	**0**	**0.121**	**0.819**
AK	**Potassium (K^+)**	**3.77**	**0.153**	**0.282**	**0**	**0.108**	**0.121**
APOC	Primary Organic Carbon	1.075	1.075	1.075	0	0	0
APNCOM	Non-carbon organic matter	0.43	0.43	0.43	0	0	0
AEC	Elementary carbon	0	0	0	0	0	0
AFE	Iron (Fe)	3.355	4.689	2.425	0	3.75	3.055
AAL	Aluminum (Al)	5.695	5.926	4.265	0	4.987	4.641
ASI	Silicon (Si)	19.425	20.739	14.929	0	17.454	16.245
ATI	Titanium (Ti)	0.28	0.312	0.337	0	0.285	0.365
AMN	Manganese (Mn)	0.115	0.0758	0.063	0	0.062	0.072
AH2O	Water (H_2O)	0.541	0.541	0.541	0	0	0
AOTHR	Unspeciated	50.219	55.345	70.002	0	0	0
ASOIL	Non-anion dust	0	0	0	95.995	64.382	72.464

ACPD
15, 35591–35643, 2015

Table 2. Heterogeneous reactions and uptake coefficients.

No.	Reaction	Uptake coefficient	References
Default heterogeneous reactions in CMAQv5.0.1			
C1	$N_2O_5 + H_2O \rightarrow 2HNO_3$	$\gamma = \begin{cases} (x_1 + x_2) \times \gamma_d^* + x_3 \times \min(\gamma_d^*, \gamma_3), & \text{RH} < \text{CRH} \\ \sum_{i=1}^{3} x_i \times \gamma_i^*, & \text{RH} > \text{IRH} \\ 0.02, & \text{otherwise} \end{cases}$ where x_1, x_2, x_3 and $\gamma_1, \gamma_2, \gamma_3$ are the normalized molar concentrations and N_2O_5 uptake coefficients on NH_4HSO_4, $(NH_4)_2SO_4$, and NH_4NO_3 respectively, $\gamma_d^* = \min(\gamma_d, 0.0124)$ where γ_d is the uptake coefficient on dry particles determined by relative humidity and temperature, RH is relative humidity, CRH is crystallization relative humidity, IRH is ice formation relative humidity determined by temperature	Davis et al. (2008)
C2	$2NO_2 + H_2O \rightarrow HONO + HNO_3$	$K = 5.0 \times 10^{-6} \times A_p$	Vogel et al. (2003)
Implemented dust heterogeneous reactions in this work			
R1	O_3 + dust → products	5.0×10^{-5}–1.0×10^{-4}	Zhu et al. (2010)
R2	OH + dust → products	0.1–1.0	Zhu et al. (2010)
R3	H_2O_2 + dust → products	1.0×10^{-4}–2.0×10^{-3}	Zhu et al. (2010)
R4	CH_3COOH + dust → products	1.0×10^{-3}	Zhu et al. (2010)
R5	CH_3OH + dust → products	1.0×10^{-5}	Zhu et al. (2010)
R6	CH_2O + dust → products	1.0×10^{-5}	Zhu et al. (2010)
R7	HNO_3 + dust → $0.5NO_3^-$ + $0.5NO_x$	1.1×10^{-3}–0.2	Dentener et al. (1996)
R8	N_2O_5 + dust → $2NO_3^-$	1×10^{-3}–0.1	Zhu et al. (2010)
R9	NO_2 + dust → NO_3^-	4.4×10^{-5}–2.0×10^{-4}	Underwood et al. (2001)
R10	NO_3 + dust → NO_3^-	0.1–0.23	Underwood et al. (2001)
R11	NO_3 + dust → HNO_3	1.0×10^{-3}	Martin et al. (2003)
R12	HO_2 + dust → $0.5H_2O_2$	0.2	Zhu et al. (2010)
R13	SO_2 + dust → SO_4^{2-}	1.0×10^{-4}–2.6×10^{-4}	Padnis and Carmichael (2000)

ACPD
15, 35591–35643, 2015

Table 3. Simulation design.

Scenario	Configuration of CMAQv5.0.1
Dust_Off	Without inline calculation of dust
Dust_Default	With default dust plume rise scheme
Dust_Revised	Revised intial friction velocity threshold constant in dust plume rise scheme
Dust_Profile	Same as Dust_Revised, but with implemented source dependent speciation profile
Dust_Chem	Same as Dust_Profile, but with implemented dust chemistry with lower limit of uptake coefficient
Dust_ChemHigh	Same as Dust_Chem, but with upper limit of uptake coefficients

ACPD
15, 35591–35643, 2015

Table 4. Evaluation statistics for tracer metals.

Dataset	Species measured	Observational frequency	Number of sites	Data source
AERONET	AOD	Daily	70 sites within our simulation domain	http://aeronet.gsfc.nasa.gov/cgi-bin/combined_data_access_new
API	PM_{10}	Daily	86 cities in China	http://datacenter.mep.gov.cn
EANET	PM_{10}, SO_2, NO_x, HNO_3, O_3	Hourly/Daily/Bi-weekly	11 sites in Japan	http://www.eanet.asia/
Fudan Univ. Obs	K^+, Mg_2^+, Ca_2^+, $PM_{2.5}$	Daily	Duolun (42.18° N, 116.48° E), Yulin (38.3° N, 109.77° E)	Huang et al. (2010)
MODIS	AOD	Daily	–	http://ladsweb.nascom.nasa.gov/data/search.html
TAQMN	PM_{10}	Daily	Xinzhuang (25.03° N, 121.43° E)	http://taqm.epa.gov.tw/taqm/en/default.aspx

ACPD
15, 35591–35643, 2015

Table 5. Evaluation statistics for tracer metals and $PM_{2.5}$.

	$PM_{2.5}$	K^+		Mg_2^+		Ca_2^+	
		Dust_Revised	Dust_Profile	Dust_Revised	Dust_Profile	Dust_Revised	Dust_Profile
Mean Obs ($\mu g m^{-3}$)	81.52	0.23		0.19		2.24	
Mean Sim ($\mu g m^{-3}$)	44.36	0.69	0.12	0.02	0.12	3.06	1.05
MB ($\mu g m^{-3}$)	−37.17	0.46	−0.11	−0.17	−0.07	0.82	−1.19
NMB (%)	−45.59	208.9	−47.83	−99.8	−36.84	36.69	−53.12
R	0.67	0.42	0.44	0.22	0.51	0.22	0.44

ACPD
15, 35591–35643, 2015

Table 6. CMAQ evaluation against EANET observations for Dust_Profile, Dust_Chem, and Dust_ChemHigh scenarios for species O_3, SO_2, SO_4^{2-}, NO_x, HNO_3, and NO_3^-.

		O_3 (ppbv)	SO_2 (ppbv)	SO_4^{2-} ($\mu g\,m^{-3}$)	NO_x (ppbv)	HNO_3 (ppbv)	NO_3^- ($\mu g\,m^{-3}$)
Mean Obs		45.81	0.59	4.38	1.75	0.43	1.52
MB	Dust_Profile	0.59	0.54	−0.71	0.63	0.46	−0.20
	Dust_Chem	−0.92	0.42	0.60	0.67	0.36	−0.03
	Dust_ChemHigh	−2.07	0.38	1.29	0.68	0.35	0.37
NMB (%)	Dust_Profile	1.26	90.70	−16.28	35.61	109.03	−13.07
	Dust_Chem	−1.97	69.83	13.74	37.79	85.17	−1.97
	Dust_ChemHigh	−4.43	63.70	29.43	38.21	81.24	24.09
R	Dust_Profile	0.63	0.68	0.79	0.69	0.65	0.71
	Dust_Chem	0.62	0.65	0.75	0.69	0.59	0.72
	Dust_ChemHigh	0.59	0.64	0.72	0.69	0.60	0.73

ACPD
15, 35591–35643, 2015

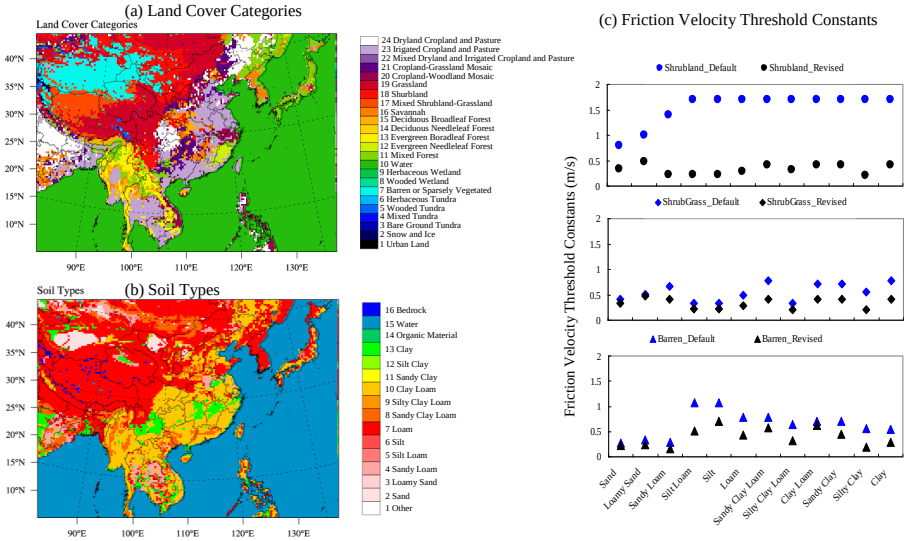

Figure 1. (a) Land cover categories, **(b)** Soil types, and **(c)** comparison of initial friction velocity threshold constants in default (blue markers) and revised (black markers) dust schemes for shrub land (top), mixed shrub and grassland (middle), and barren or sparsely vegetated (bottom) land cover.

ACPD
15, 35591–35643, 2015

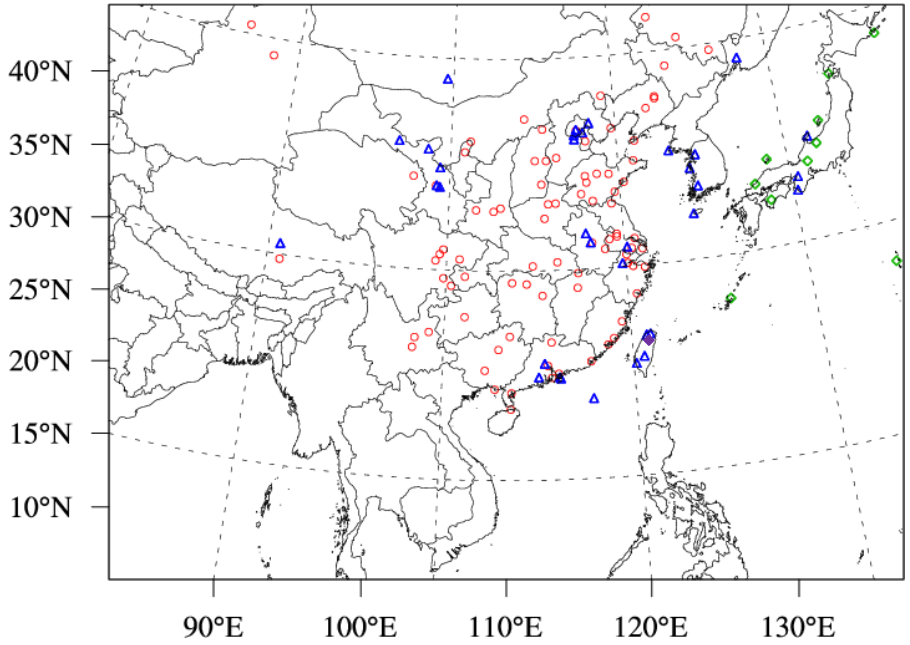

Figure 2. Modeling domain and locations of observation stations from Fudan observation network (orange rectangles), API (red circles), AERONET (blue triangles), EANET (green diamonds), and TAQMN (purple diamonds) over East Asia.

ACPD
15, 35591–35643, 2015

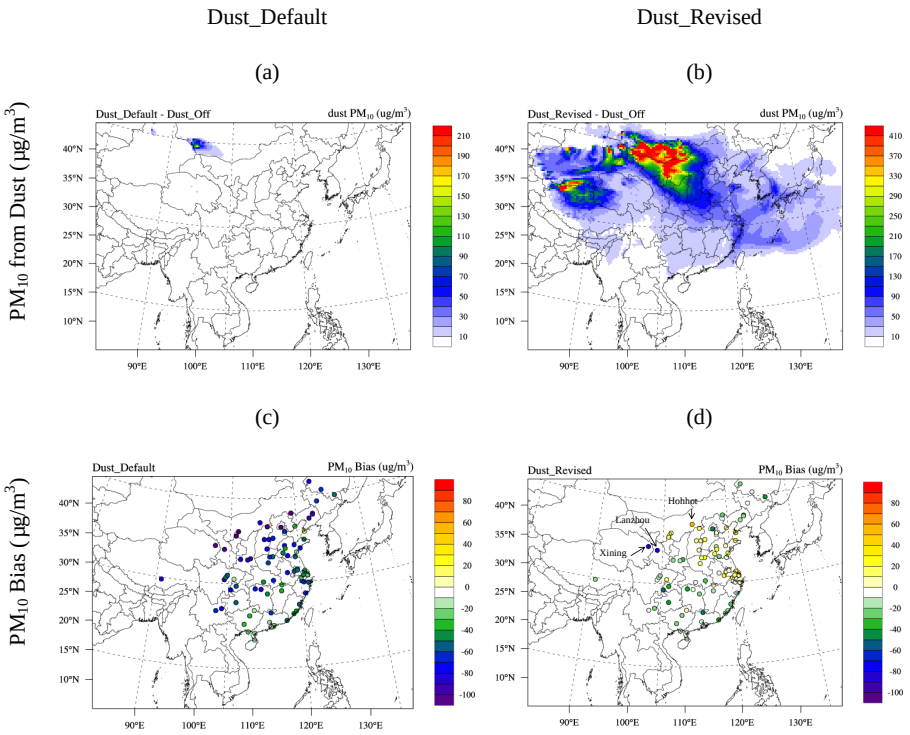

Figure 3. PM_{10} concentration difference from **(a)** Dust_Default – Dust_Off, and **(b)** Dust_Revised – Dust_Off. PM_{10} simulation bias against observation at API stations for **(c)** Dust_Default and **(d)** Dust_Revised scenarios.

ACPD
15, 35591–35643, 2015

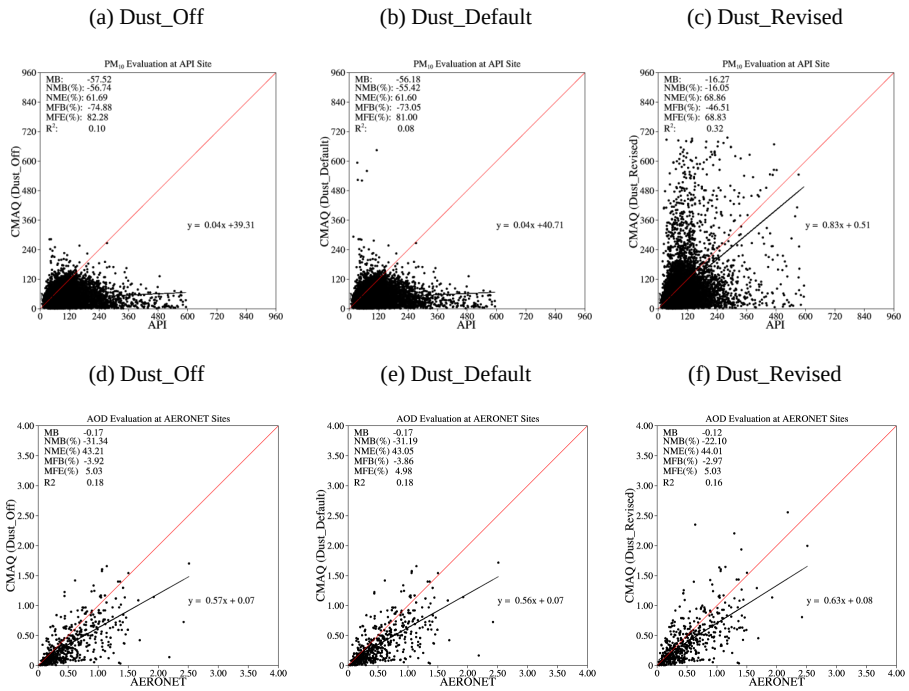

Figure 4. CMAQ evaluation against PM_{10} from API (upper row) and AOD (bottom row) from AERONET for Dust_Off (left column), Dust_Default (middle column), and Dust_Revised (right column) scenarios. Formula of calculating evaluation statistics including mean bias (MB), normalized mean bias (NMB), normalized mean error (NME), mean fractional bias (MFB), mean fractional error (MFE), and correlation coefficient (R) can be found in Dong et al. (2013).

ACPD
15, 35591–35643, 2015

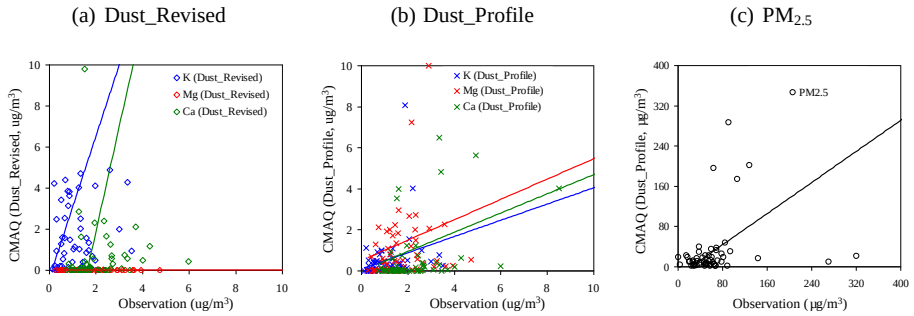

Figure 5. Model evaluations of CMAQ simulated metal tracers against observations from Fudan University at Duolun and Yulin for **(a)** Dust_Revised and **(b)** Dust_Profile scenarios. Note that simulations and observations of K^+ and Mg_2^+ are upscaled by 5 and 10 times, respectively, to make them comparable with Ca_2^+ in the same plot. Right column is the evaluation of CMAQ simulated **(c)** $PM_{2.5}$ at Duolun and Yulin.

ACPD
15, 35591–35643, 2015

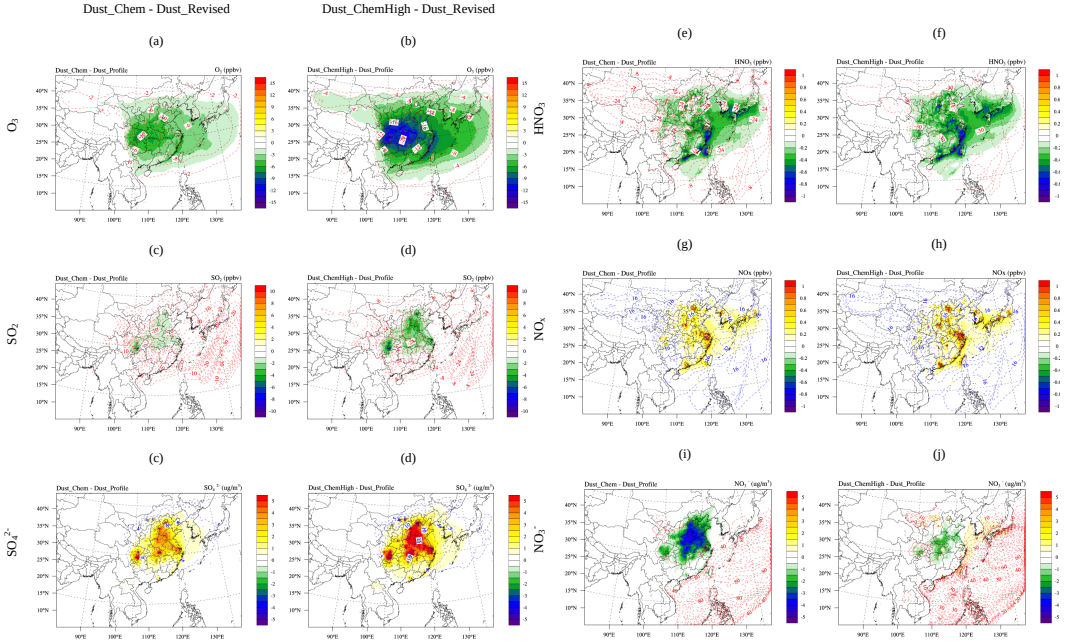

Figure 6. Five-year averages for March and April from 2006 to 2010 of dust heterogeneous chemistry impacts with lower (left column) and upper (right column) uptake coefficients, for species O_3 (1st row), SO_2 (2nd row), SO_4^{2-} (3rd row), HNO_3 (4th row), NO_x (5th row), and NO_3^- (6th row). Color contours represent the absolution concentration changes, and dash contour lines with numbers indicate the percentage changes.

ACPD
15, 35591–35643, 2015

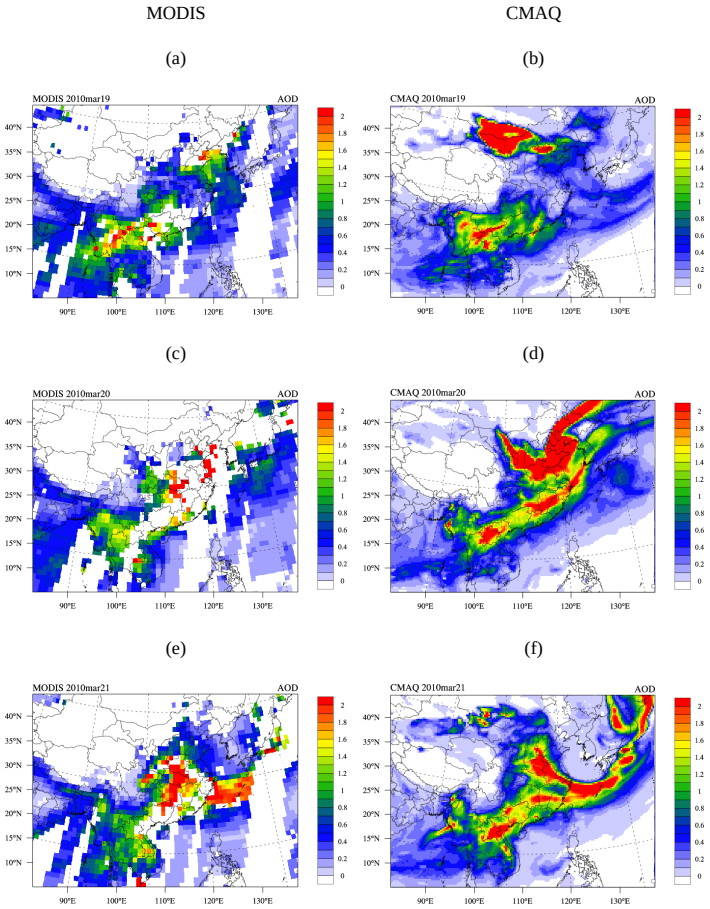

Figure 7. Daily MODIS observed (left column) and CMAQ simulated AOD (right column) for 19 March (top row), 20 March (middle row), and 21 March (bottom row).

ACPD
15, 35591–35643, 2015

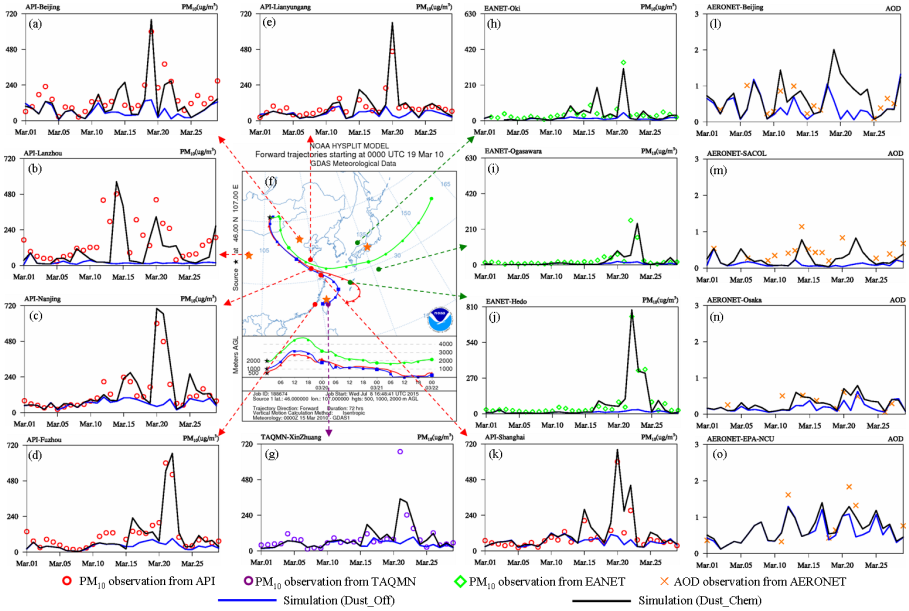

Figure 8. Forward trajectories from **(f)** HYSPLIT, and temporal variations of PM_{10} and AOD on a daily scale. Comparison between simulated (black lines for Dust_Chem scenario, and blue lines for Dust_Off scenario) and observed PM_{10} from API (red circles) at **(a)** Beijing, **(b)** Lanzhou, **(c)** Nanjing, **(d)** Xiamen, **(e)** Lianyungang, and **(k)** Shanghai. Comparison between simulations and observed PM_{10} from TAQMN (purple circles) at **(g)** Xinzhuang. Comparison between simulations and observed AOD from EANET (green diamonds) at **(l)** Beijing, **(m)** SACOL, **(n)** Osaka, and **(o)** NCU. Locations of cities or stations are indicated by the tails of arrow lines (for PM_{10}) or orange stars (for AOD).

ACPD
15, 35591–35643, 2015

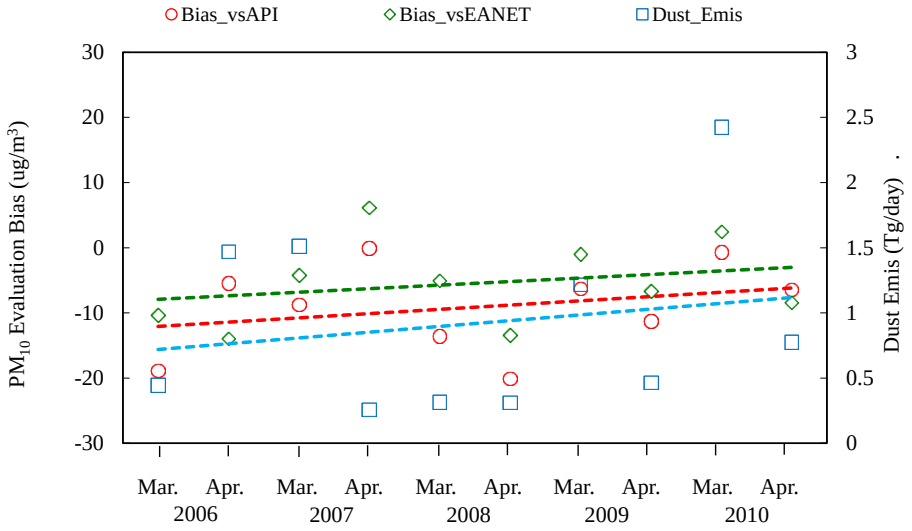

Figure 9. CMAQ predictions of dust emission rate (solid orange rectangles), and simulation bias of PM_{10} against observations from API (red circles) and EANET (green diamonds). Dash lines indicated the trends of the variables.

ACPD
15, 35591–35643, 2015

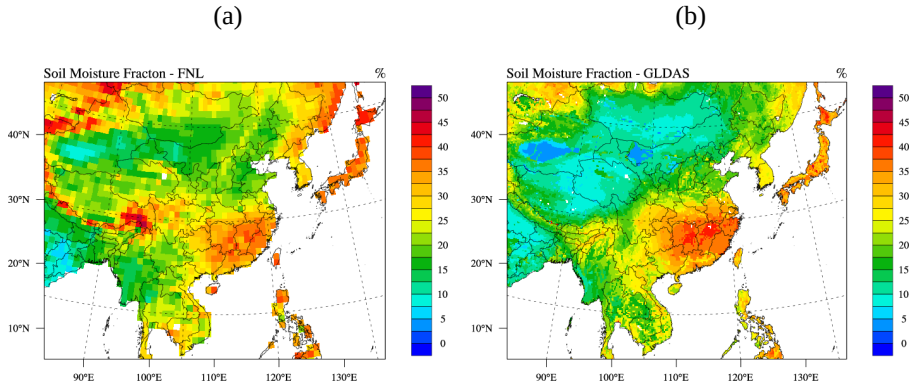

Figure 10. Five-year averages (for March and April) of soil moisture fraction in top 10 cm soil depth from **(a)** FNL and **(b)** GLDAS.

ACPD
15, 35591–35643, 2015